THE UNIVERSITY OF QUEENSLAND AUSTRALIA | CREATE CHANGE

Higher, faster, smaller: Pushing the limits of fMRI at ultra-high field

Saskia Bollmann

Centre for Advanced Imaging, The University of Queensland, Brisbane, Australia

Acknowledgement of **Country**

The University of Queensland (UQ) acknowledges the Traditional Owners and their custodianship of the lands on which we meet.

We pay our respects to their Ancestors and their descendants, who continue cultural and spiritual connections to Country.

We recognise their valuable contributions to Australian and global society.

Introduction

- ‘Higher’ — fMRI at 7T offers multiple advantages
  - Higher signal-to-noise ratio (SNR)[1,2,3]

7T: 12 ml = 2x2x3mm^3

3T: 48 ml = 4x4x3mm^3

1.5T: 75 ml = 5x5x3mm^3

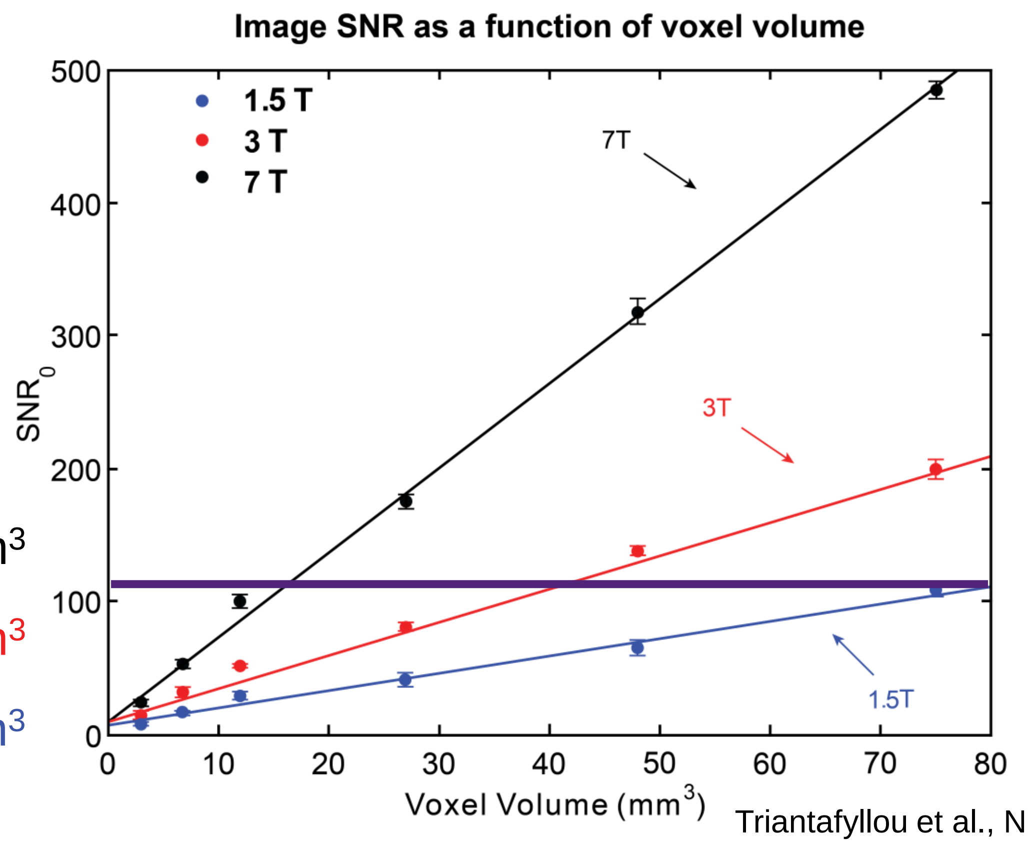

Triantafyllou et al., NI, 2005

[1]Edelstein, 1986; [2]Pohmann, 2016; [3]Triantafyllou, 2005; [4]Gati, 1997; [5]Okada, 2005; [6]van der Zwaag, 2009; [7]Pruessmann, 1999; [8]Wald, 2012, [9]Hillmann, 2104; [10]Iadecola, 2017; [11]Hillman, 2007; [12]Ts’o, 1990; [13]Norris, 2006; [14]Tian, 2010; [15]Gagnon, 2015

Introduction

- ‘Higher’ — fMRI at 7T offers multiple advantages
  - Higher signal-to-noise ratio (SNR)[1,2,3]
  - Higher functional contrast[4,5,6]

7T ~ 5 %

3T ~ 3 %

1.5T < 1%

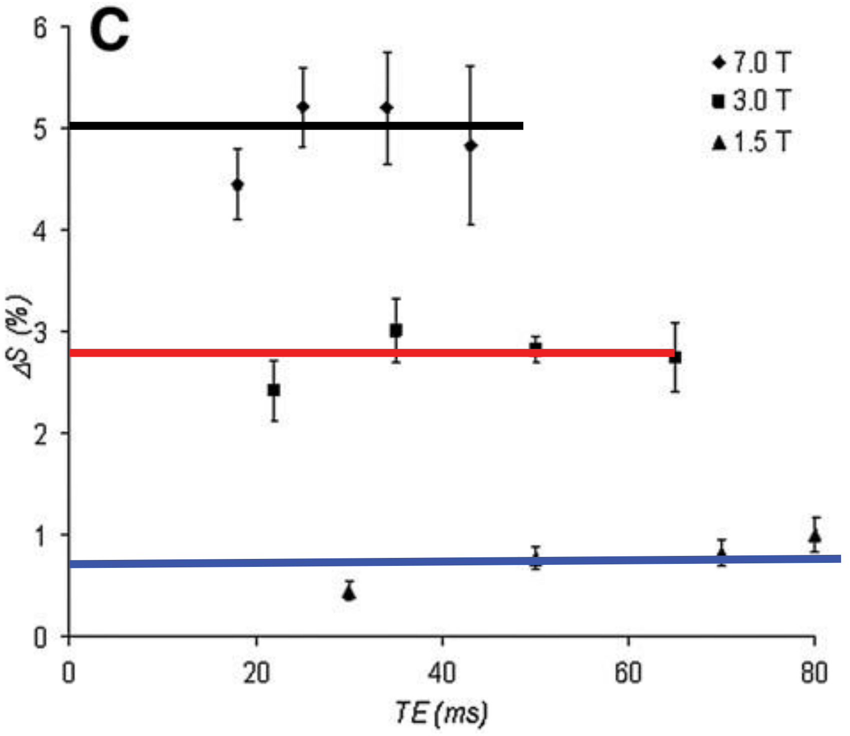

van der Zwaag et al., NI, 2009

[1]Edelstein, 1986; [2]Pohmann, 2016; [3]Triantafyllou, 2005; [4]Gati, 1997; [5]Okada, 2005; [6]van der Zwaag, 2009; [7]Pruessmann, 1999; [8]Wald, 2012, [9]Hillmann, 2104; [10]Iadecola, 2017; [11]Hillman, 2007; [12]Ts’o, 1990; [13]Norris, 2006; [14]Tian, 2010; [15]Gagnon, 2015

Introduction

- 'Higher' — fMRI at 7T offers multiple advantages
  - Higher signal-to-noise ratio (SNR)[1,2,3]
  - Higher functional contrast[4,5,6]
  - More acceleration[7,8]

Ultimate g-factor

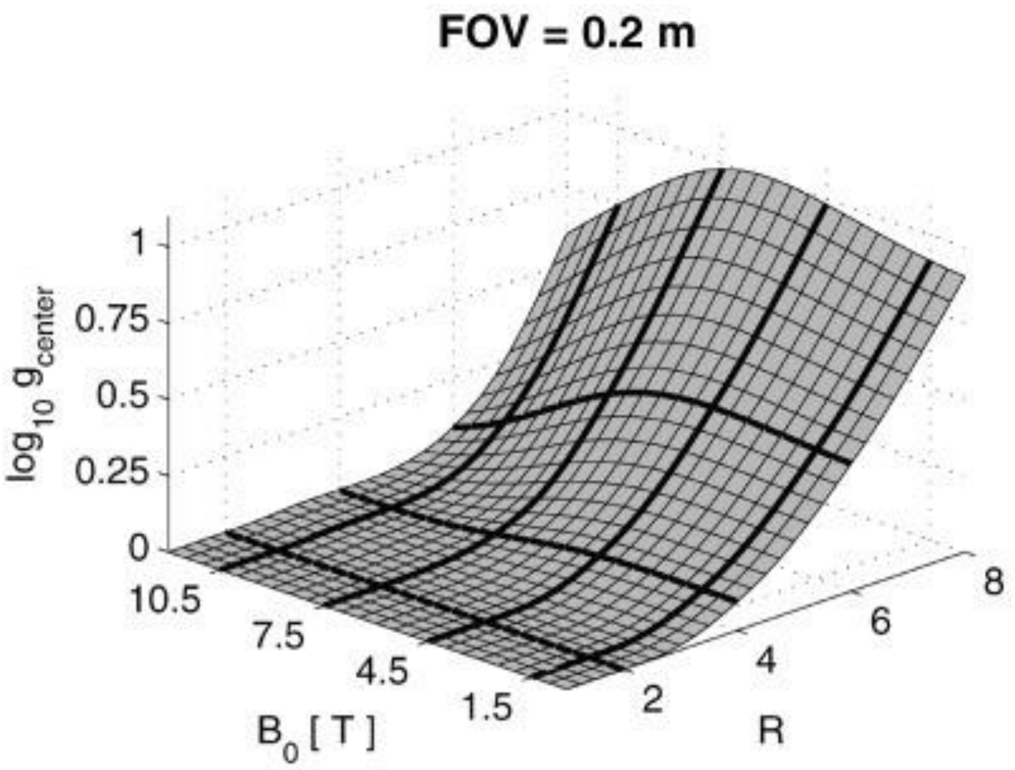

Wiesinger et al., MRM, 2004

[1]Edelstein, 1986; [2]Pohmann, 2016; [3]Triantafyllou, 2005; [4]Gati, 1997; [5]Okada, 2005; [6]van der Zwaag, 2009; [7]Pruessmann, 1999; [8]Wald, 2012, [9]Hillmann, 2104; [10]Iadecola, 2017; [11]Hillman, 2007; [12]Ts'o, 1990; [13]Norris, 2006; [14]Tian, 2010; [15]Gagnon, 2015

Introduction

- ‘Higher’ — fMRI at 7T offers multiple advantages
  - Higher signal-to-noise ratio (SNR)[1,2,3]
  - Higher functional contrast[4,5,6]
  - More acceleration[7,8]
- ‘Smaller’ — neurovascular responses are tightly controlled[9,10]
  - Evidence of depth-dependent[11] and topographic[12] hemodynamic specificity

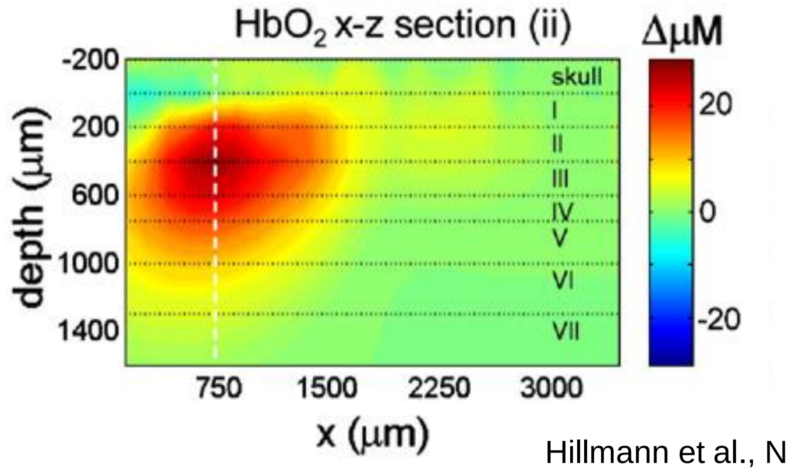

Hillmann et al., NI, 2007

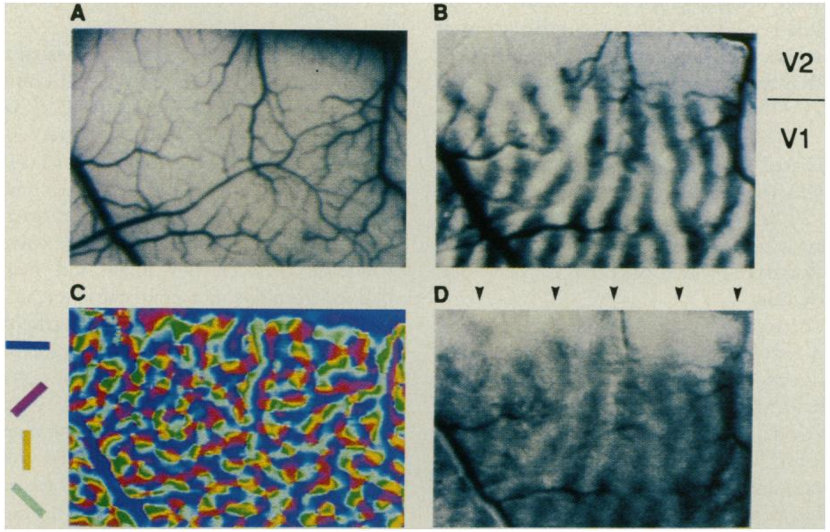

Ts’o et al., 1990

[1]Edelstein, 1986; [2]Pohmann, 2016; [3]Triantafyllou, 2005; [4]Gati, 1997; [5]Okada, 2005; [6]van der Zwaag, 2009; [7]Pruessmann, 1999; [8]Wald, 2012, [9]Hillmann, 2104; [10]Iadecola, 2017; [11]Hillman, 2007; [12]Ts’o, 1990; [13]Norris, 2006; [14]Tian, 2010; [15]Gagnon, 2015

Introduction

- ‘Higher’ — fMRI at 7T offers multiple advantages
  - Higher signal-to-noise ratio (SNR)[1,2,3]
  - Higher functional contrast[4,5,6]
  - More acceleration[7,8]
- ‘Smaller’ — neurovascular responses are tightly controlled[9,10]
  - Evidence of depth-dependent[11] and topographic[12] hemodynamic specificity
- ‘Faster’ — immediate neurovascular responses[9,10]
  - Time to peak ~ 5 seconds[13]
  - Response onset < 500 ms[11,14,15]

Deoxy-hemoglobin

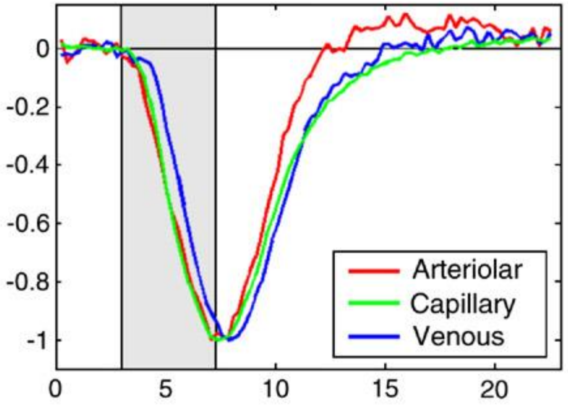

Hillmann et al., 2007

Arteriolar diameter change

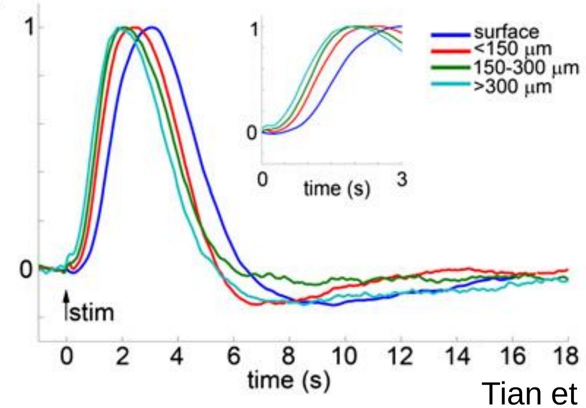

Tian et al., 2010

[1]Edelstein, 1986; [2]Pohmann, 2016; [3]Triantafyllou, 2005; [4]Gati, 1997; [5]Okada, 2005; [6]van der Zwaag, 2009; [7]Pruessmann, 1999; [8]Wald, 2012, [9]Hillmann, 2104; [10]Iadecola, 2017; [11]Hillman, 2007; [12]Ts’o, 1990; [13]Norris, 2006; [14]Tian, 2010; [15]Gagnon, 2015

Pushing the limits of fMRI at ultra-high field

Spatial and temporal correlations
Dynamic stimuli
Topographic analyses
Depth-dependent analyses

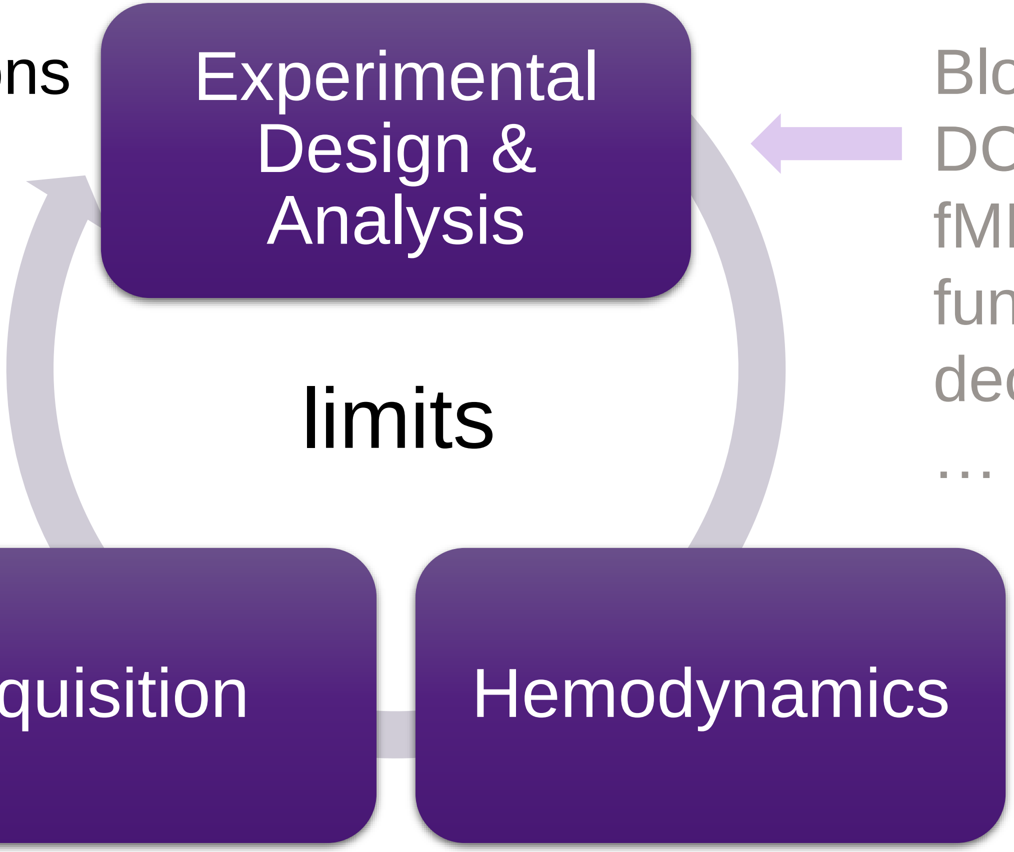

Block designs, (layer) DCMs, physiology, EEG-fMRI, time-varying functional connectivity, deconvolution, modelling …

SMS, 3D EPI,
spirals, t-hex, MREG,
line scanning,
B_0, gradients, coils,
shims, field monitoring, …

pial bias,
fMRI contrast
mechanisms,
…

Fast fMRI

Acquisition: Echo-Planar Imaging (EPI)

Echo-Planar Imaging (EPI)[1]

- One slice is excited and the complete 2D k-space is read out in a couple of tens of milliseconds

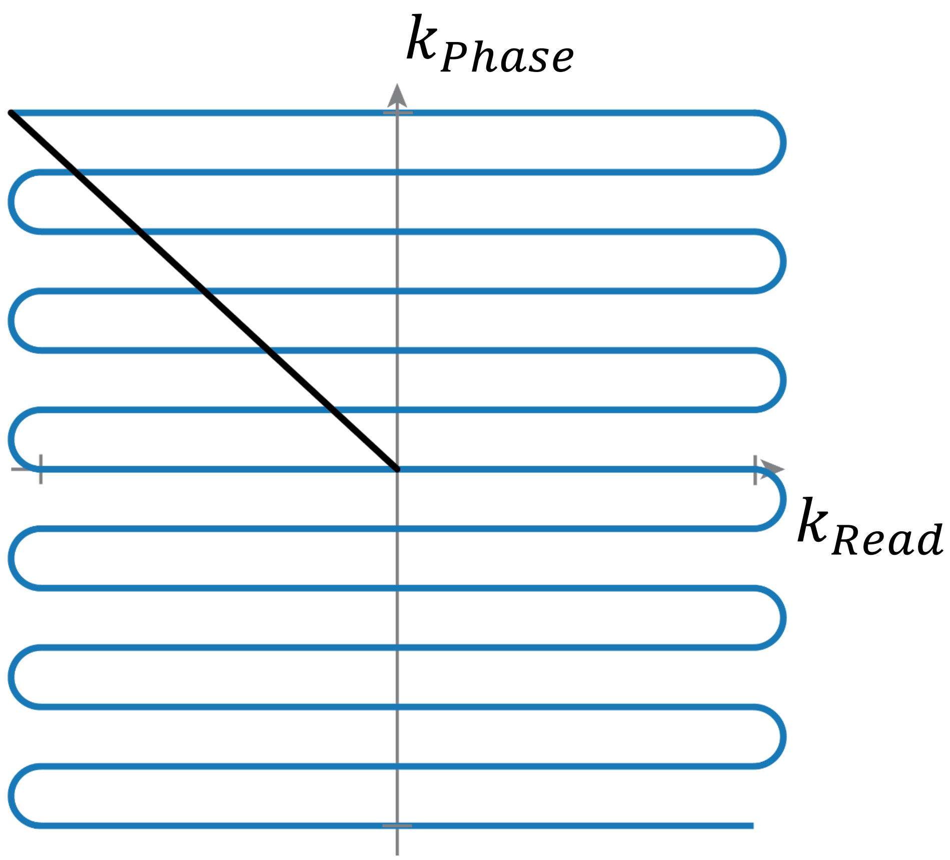

Weisskoff et al., 1993, SMRM

TR ~ 133 ms
(1 slice)

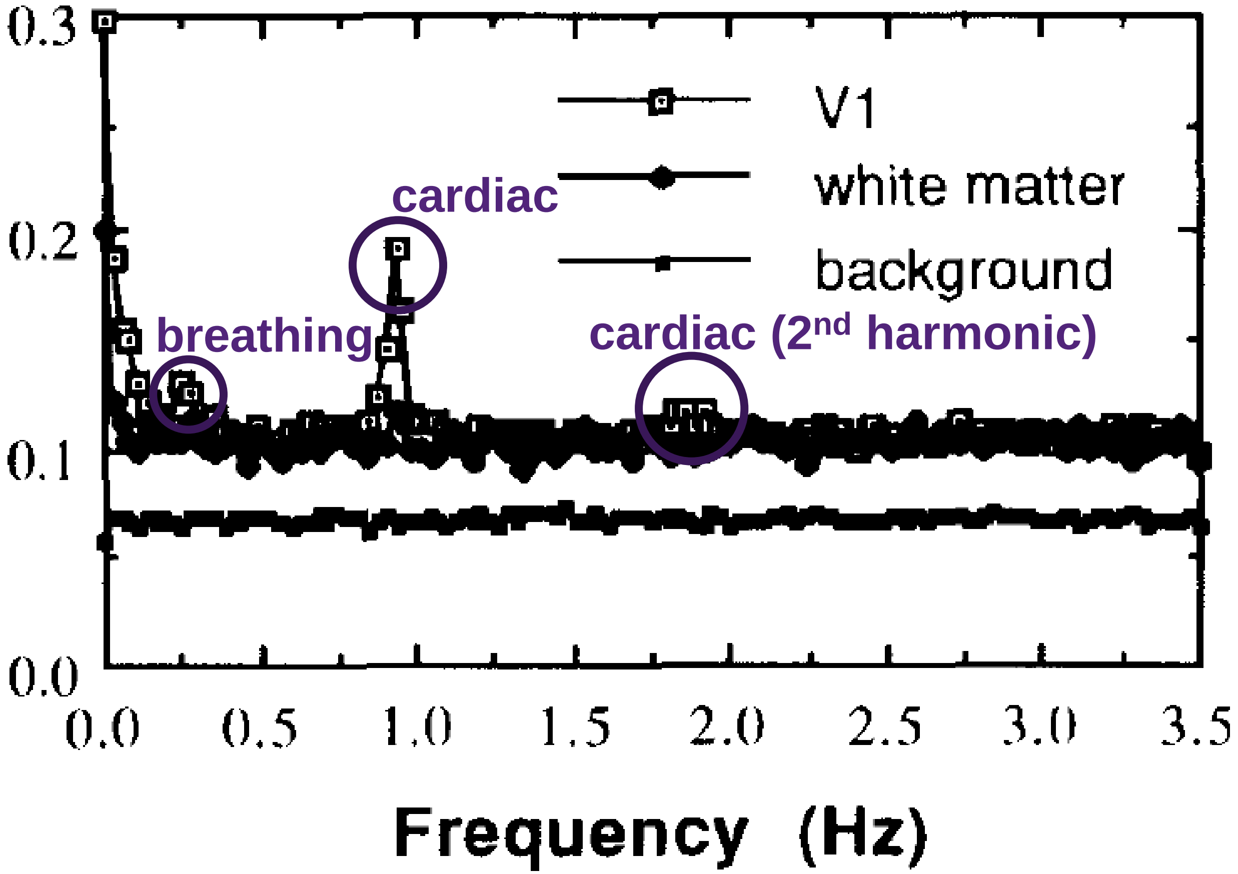

[1]Mansfield, 1977, J Phys C Solid State Phys

Fast fMRI

Acquisition: Simultaneous Multislice (SMS)

Simultaneous Multislice (SMS) / Multiband[1,2]

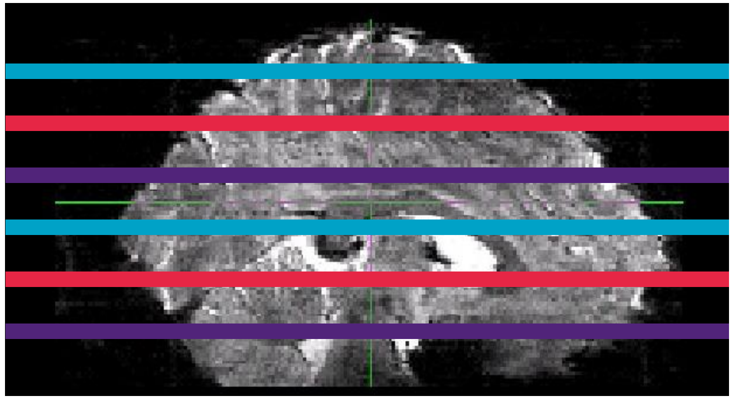

Uğurbil, 2013, NI

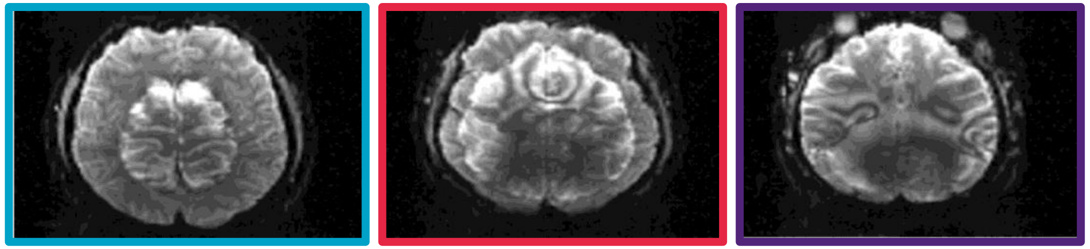

[1]Maudsley, 1980, JMR; [2]Müller, 1988, MRM; [3]Larkman et al., 2001, JMRI; [4]Breuer et al., 2005, MRM, [5]Setsompop et al., 2012, MRM

Simultaneous Multislice (SMS) / Multiband[1,2,3]

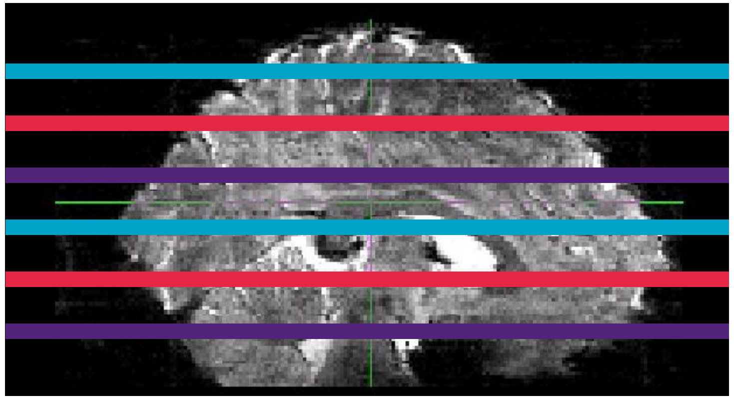

Uğurbil, 2013, NI

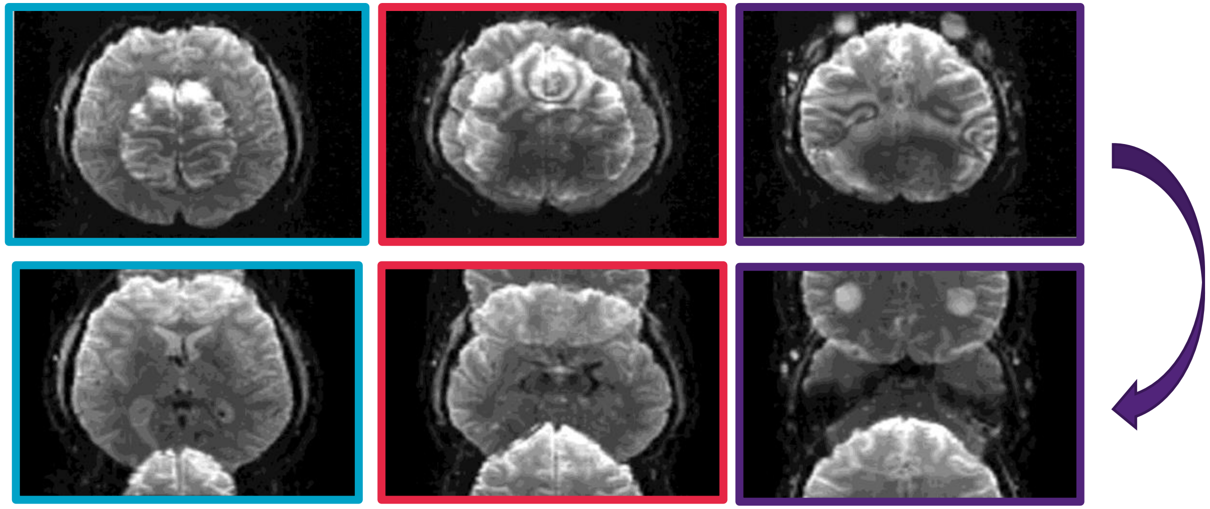

CAIPIRINHA[4]

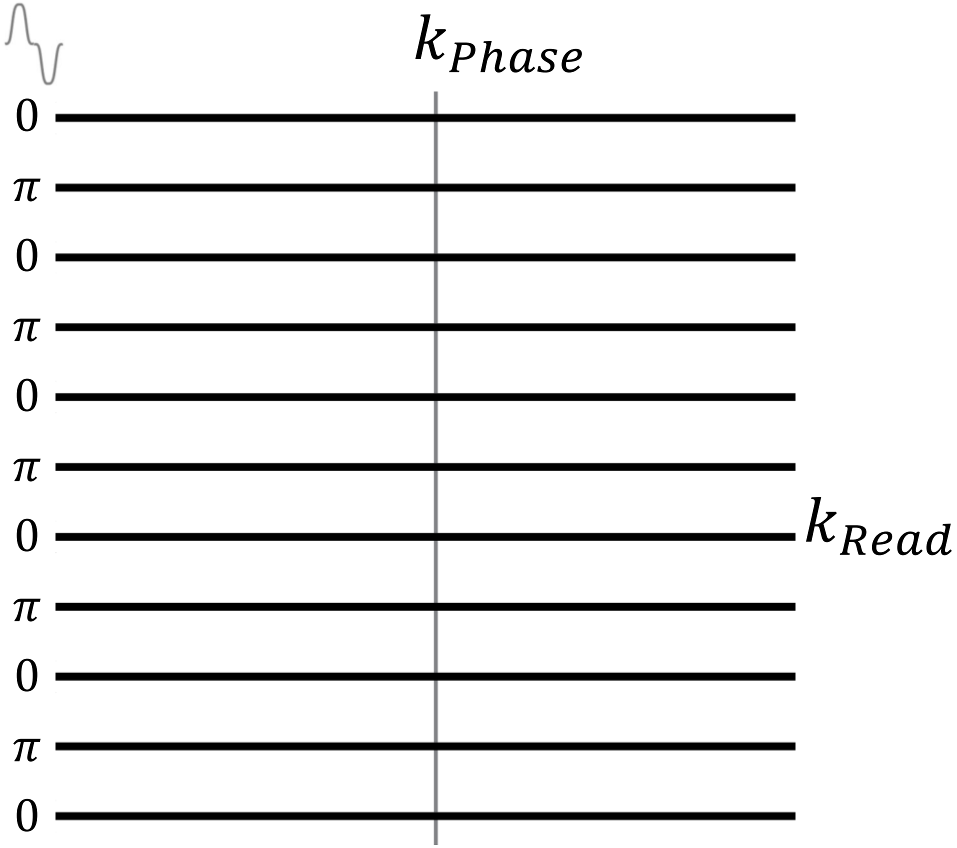

linear phase in k-space ⟷ (FT) shift in image space

[1]Maudsley, 1980, JMR; [2]Müller, 1988, MRM; [3]Larkman et al., 2001, JMRI; [4]Breuer et al., 2005, MRM, [5]Setsompop et al., 2012, MRM

Simultaneous Multislice (SMS) / Multiband[1,2,3]

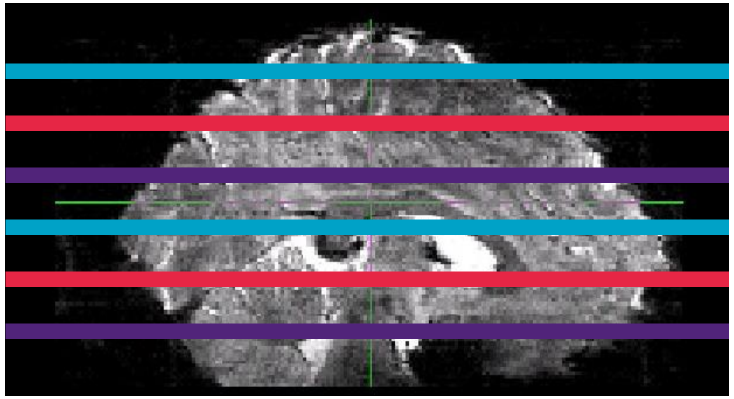

Uğurbil, 2013, NI

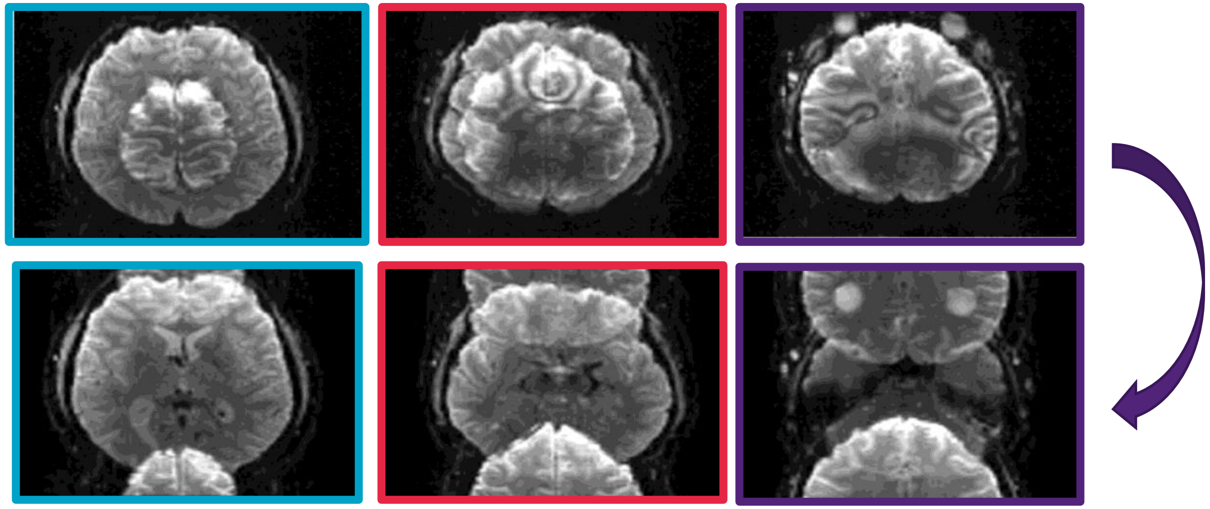

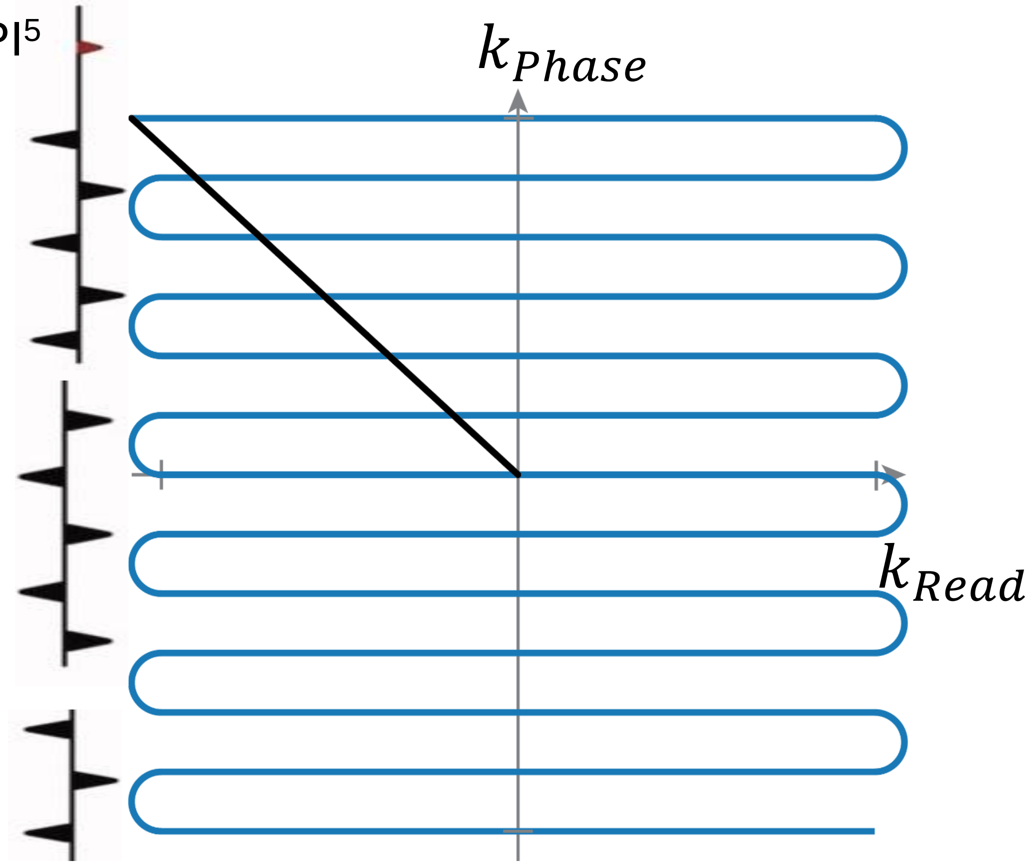

linear phase in k-space ⟷ (FT) shift in image space

[1]Maudsley, 1980, JMR; [2]Müller, 1988, MRM; [3]Larkman et al., 2001, JMRI; [4]Breuer et al., 2005, MRM; [5]Setsompop et al., 2012, MRM

Simultaneous Multislice (SMS) / Multiband – Success

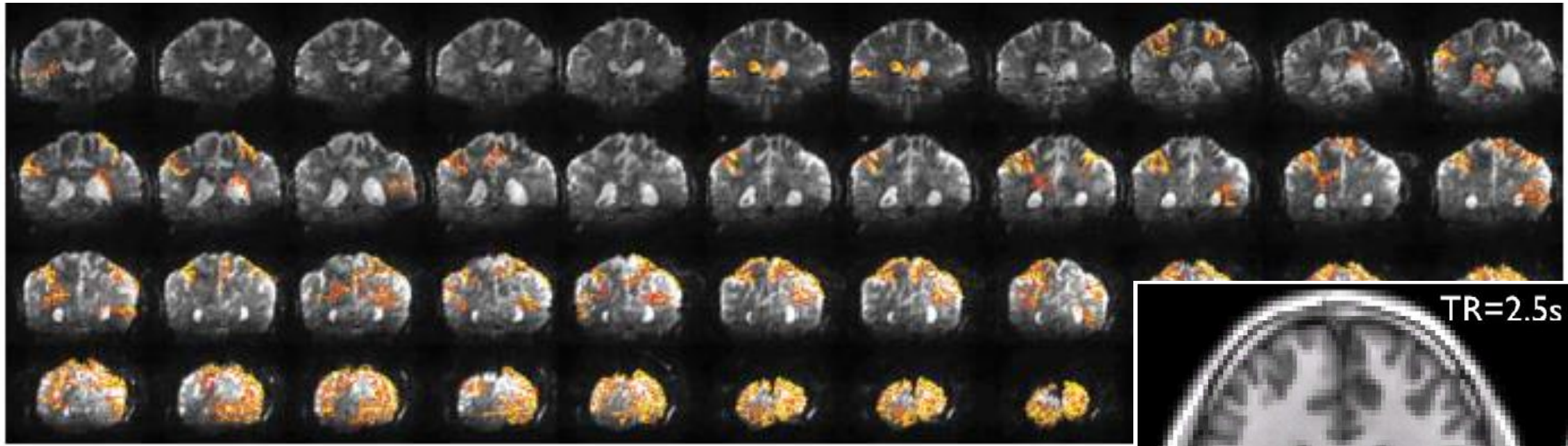

Moeller et al., 2010, MRM

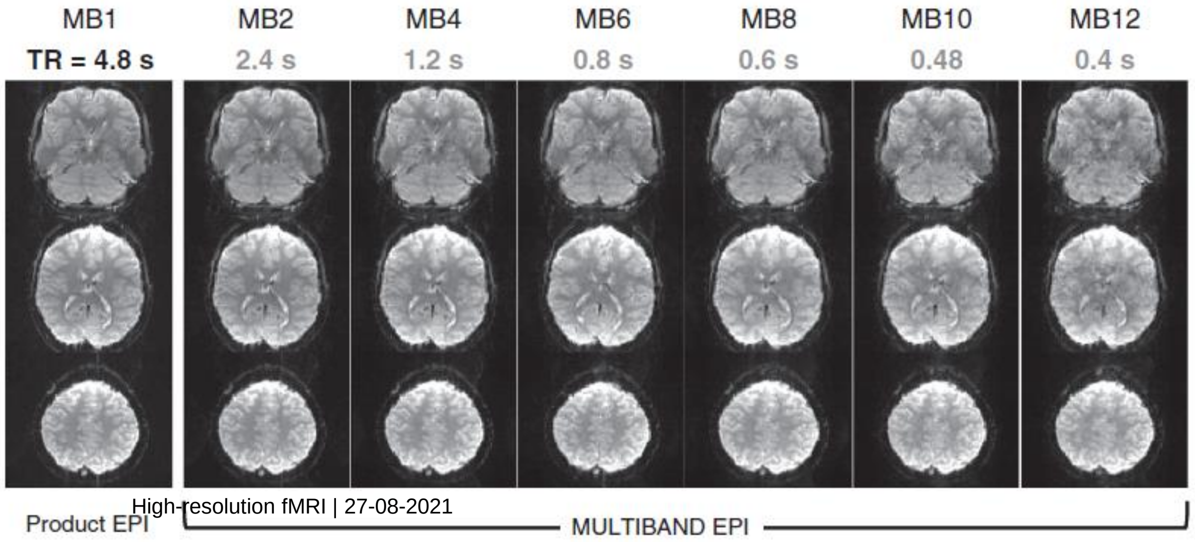

Uğurbil et al., 2013, NI

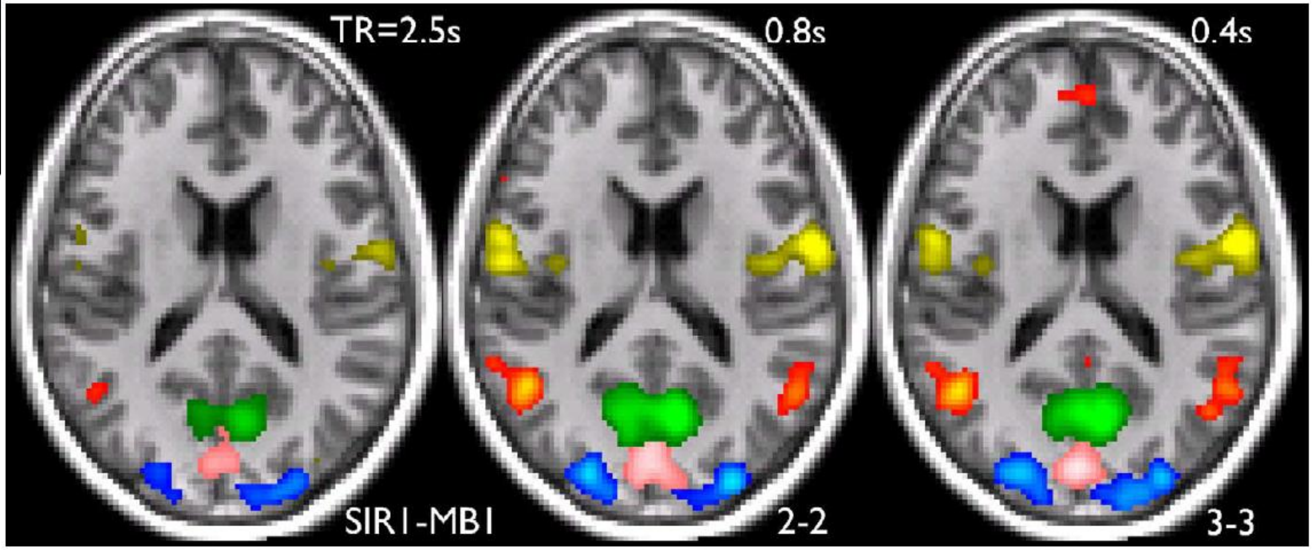

Feinberg et al., 2010, PLoS ONE

Simultaneous Multislice (SMS) / Multiband – Summary

Advantages

- Increased SNR efficiency ($\sqrt{N}$)
- Increased sampling rate

Disadvantages

- g-factor penalty
- Slice-leakage

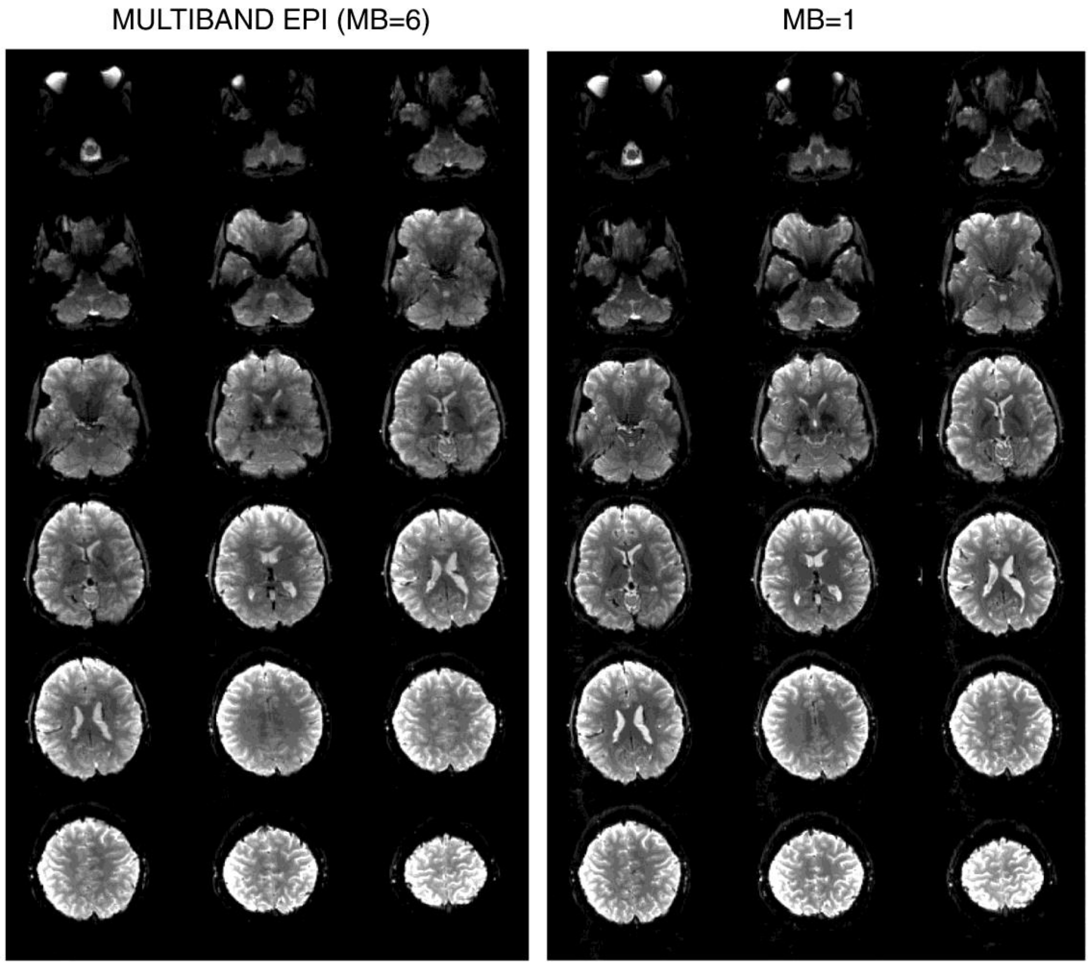

Uğurbil, 2013, NI

Fast fMRI

Analysis: Spatial correlations

False-Positive Activation due to Signal Leakage between Simultaneously Excited Slices

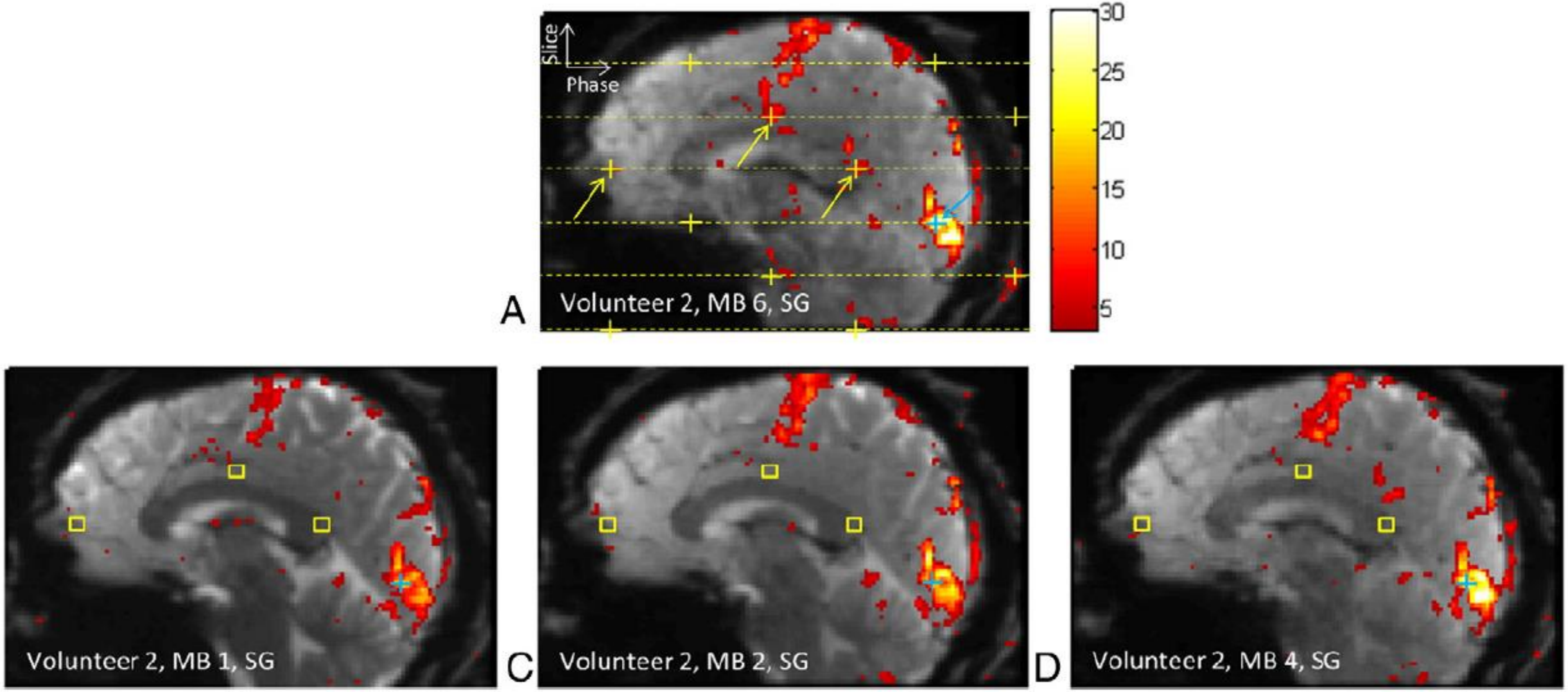

Todd et al., 2016, NI

@ 3T with 32-channel coil, GRAPPA 2

Strong Variability in Resting-State Networks at High Acceleration Factors

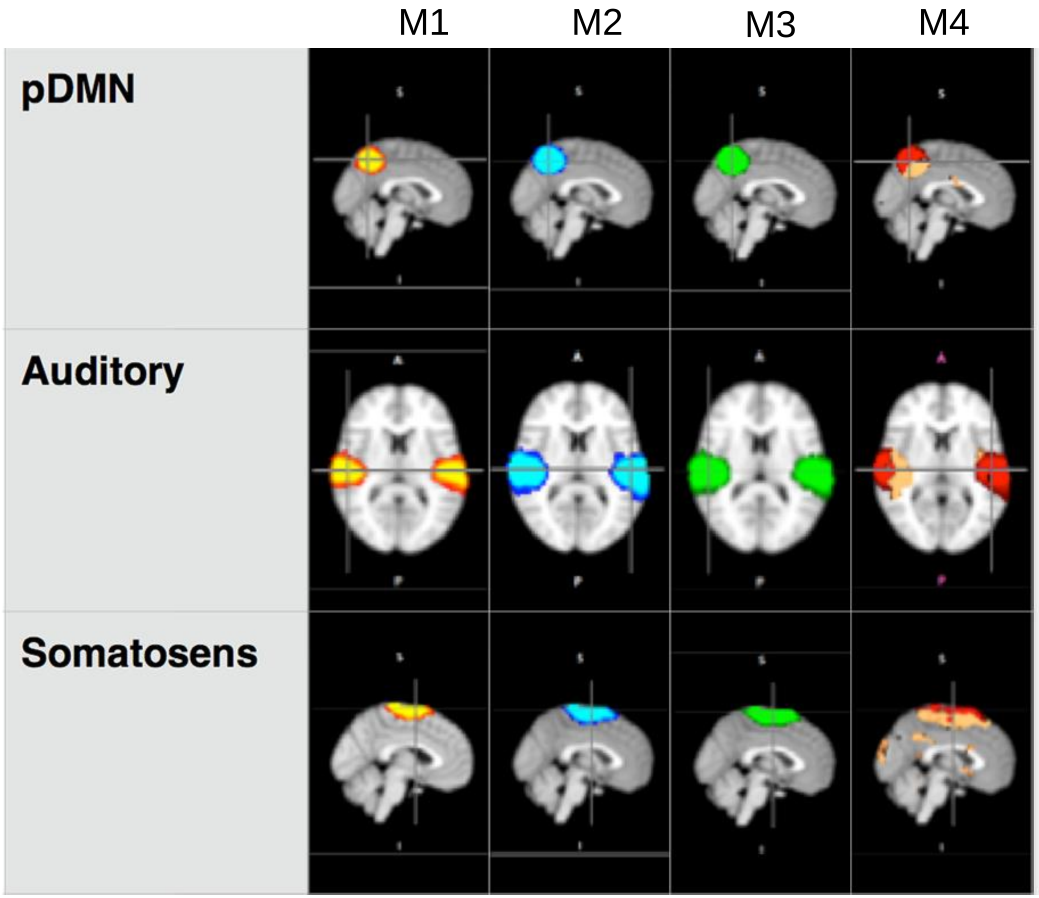

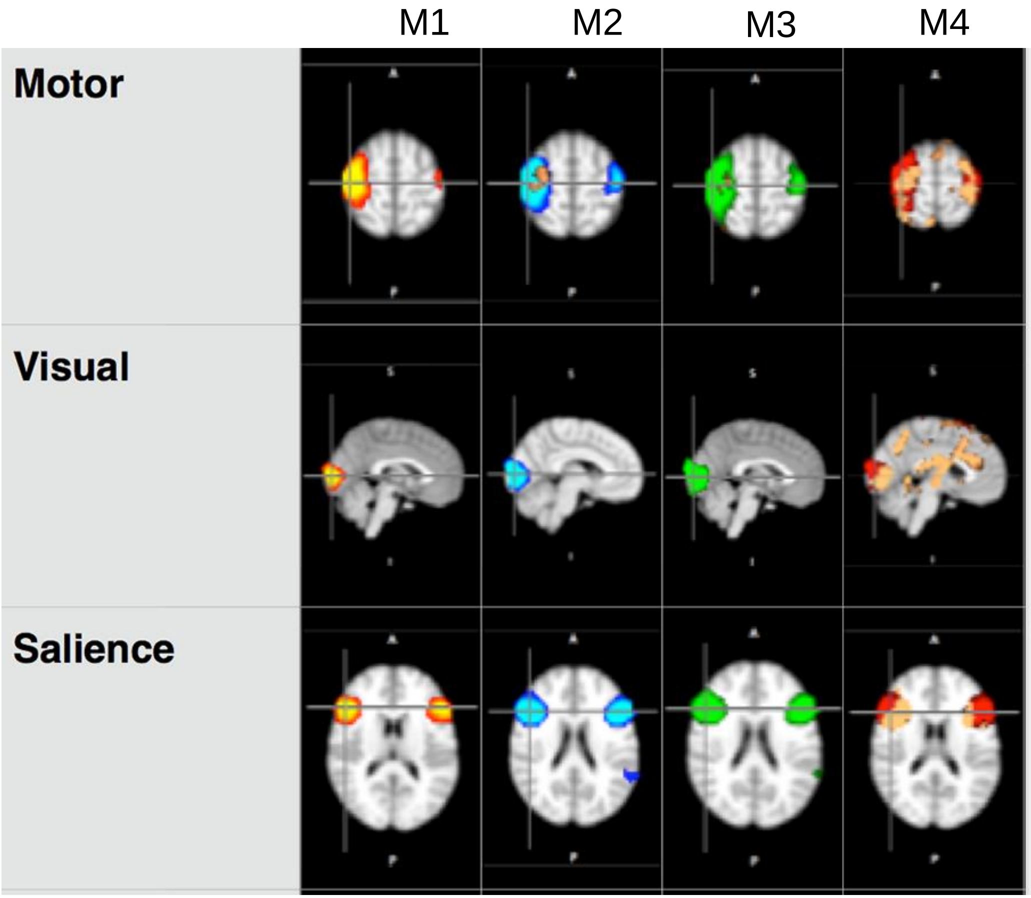

Preibisch et al., 2015, PLOS One

@ 3T with 32-channel coil, SENSE 2

Slice-Leakage in the HCP 100 Release[1]

81 out of 96

motor task

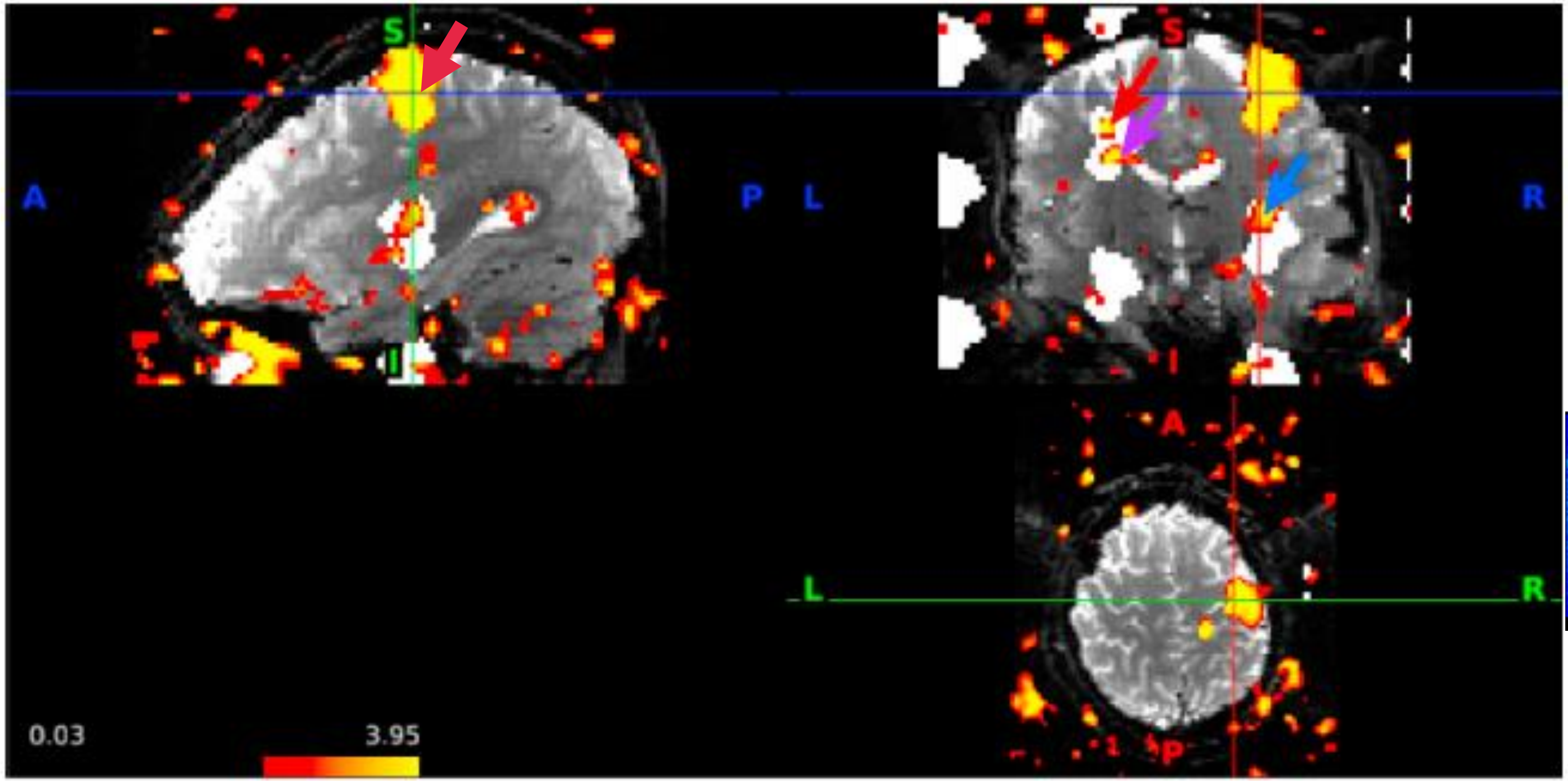

As much acceleration as necessary, as little as possible!

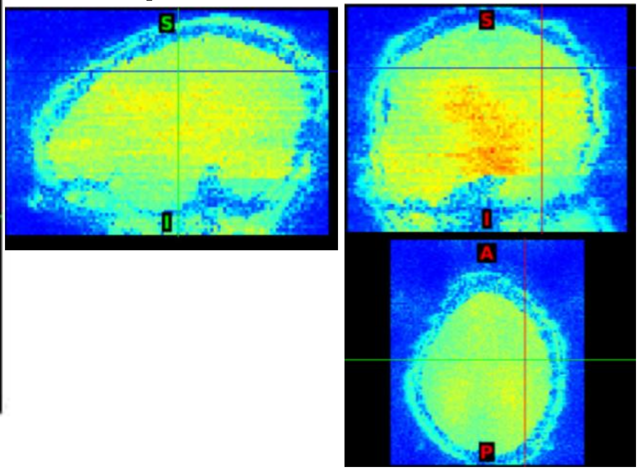

Split slice-GRAPPA[2] necessary to reduce slice leakage

@ 3T with 32-channel coil

[1]Risk et al., 2018, NI; [2]Cauley et al., 2014, MRM

Fast fMRI

Analysis: Temporal correlations

The University of Queensland Australia | Create Change

Temporal (Serial, Auto)-Correlation of the Noise

- Increased number of sampling points does not increase the degrees of the freedom at the same rate, because of serial correlations in the noise[1]

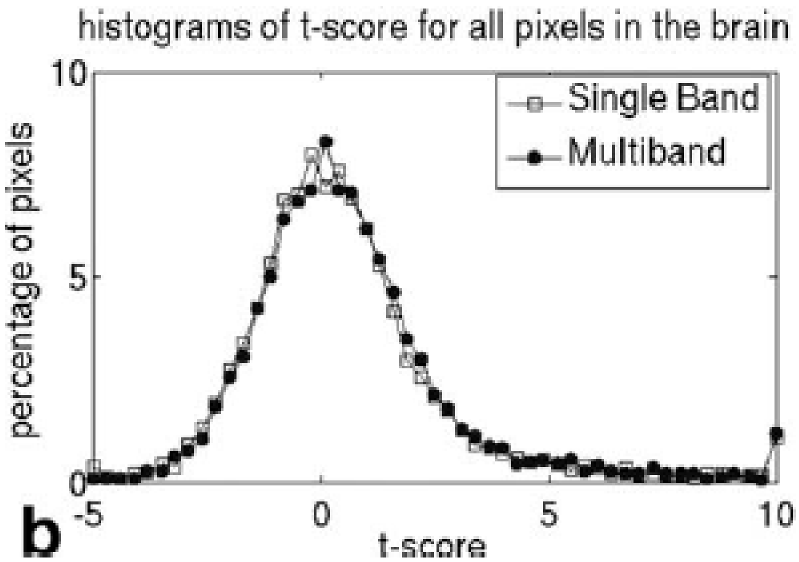

Moeller et al., 2010, MRM;
Same TR and number of volumes

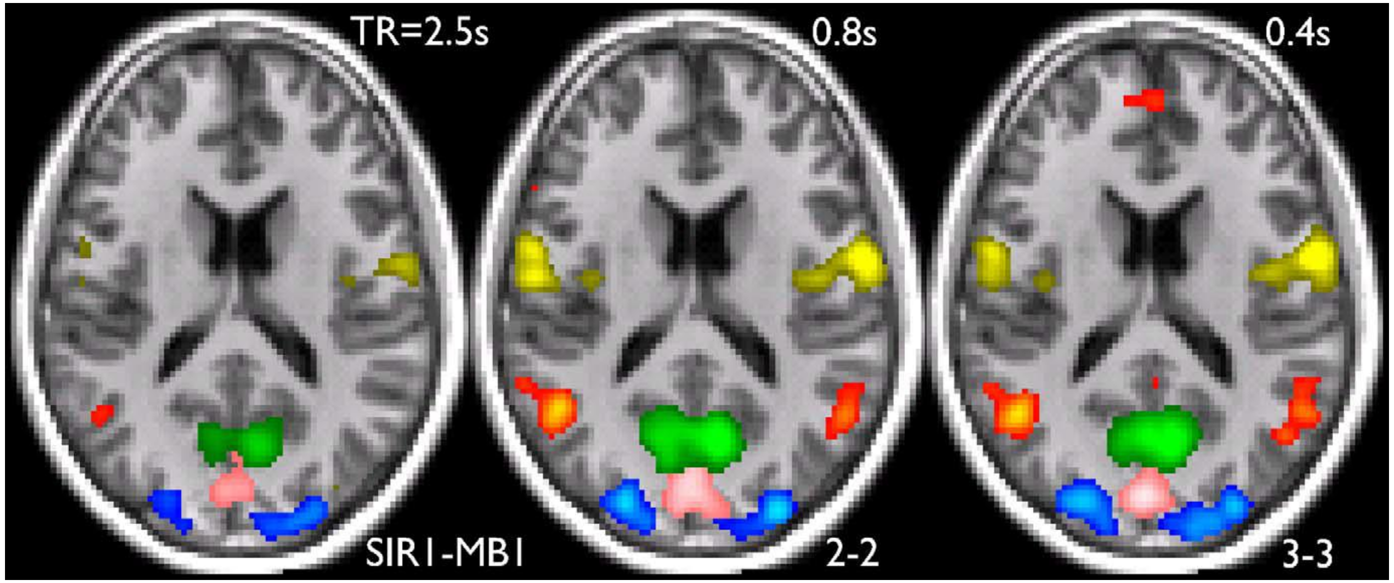

Feinberg et al., 2010, PloS ONE;
Mixture-modelling

[1]Worsley and Friston, 1995, NI;

Increased false-positive rates[1,2,3,4,5]

Chen et al., 2019, NI

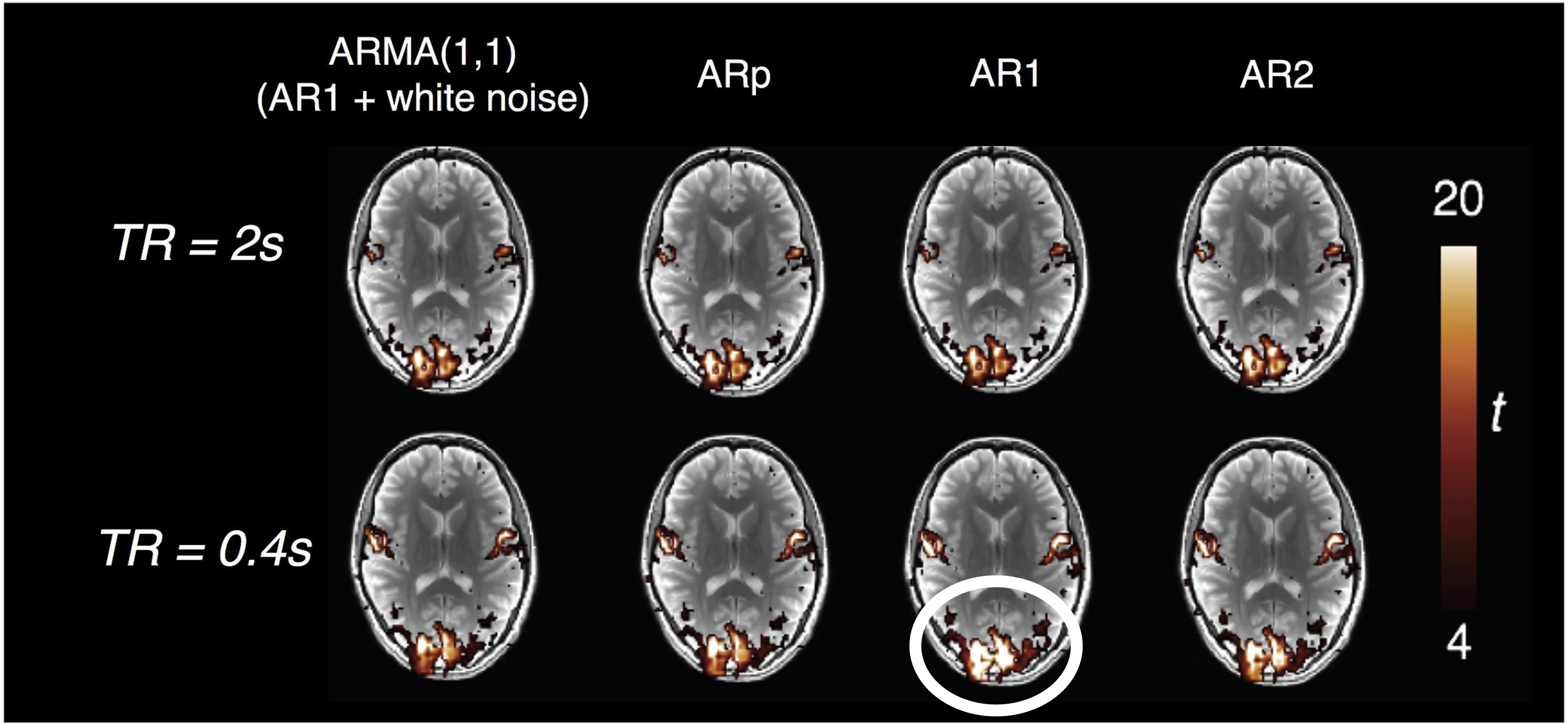

[1]Eklund et al., 2012, NI; [2]Sahib et al., 2016, MRM; [3]Bollmann et al., 2018, NI; [4]Corbin et al., 2018, HBM; [5]Olszowy et al., 2019, Nat Com

THE UNIVERSITY OF QUEENSLAND AUSTRALIA

Noise Spectrum in Fast Acquisitions

TR = 2356 ms

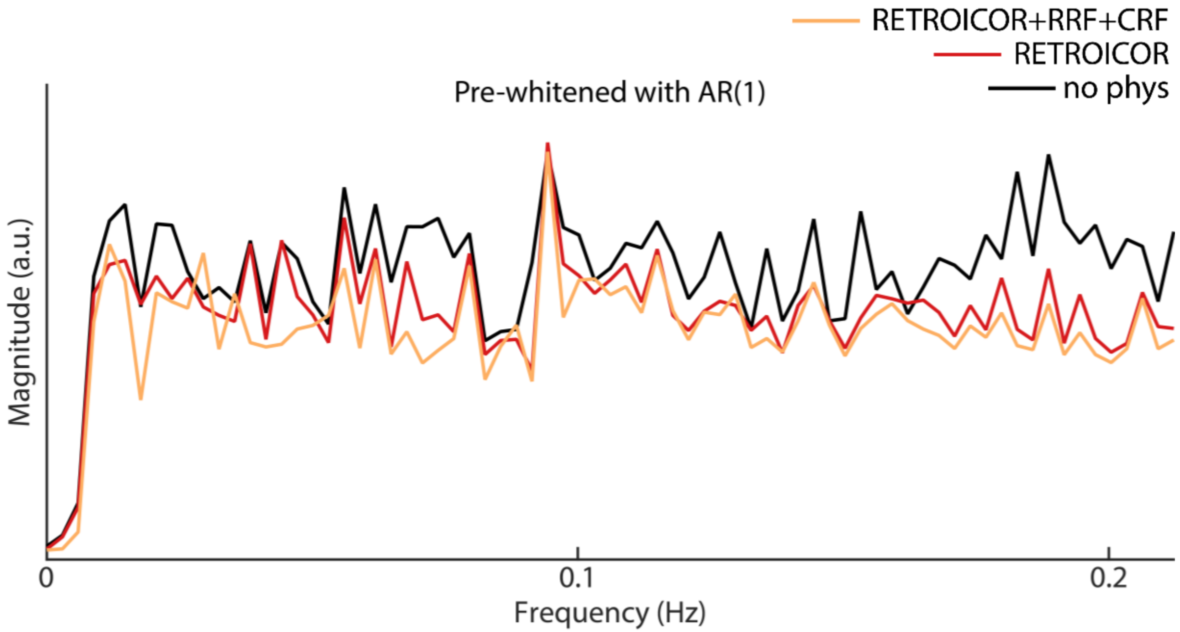

TR = 589 ms

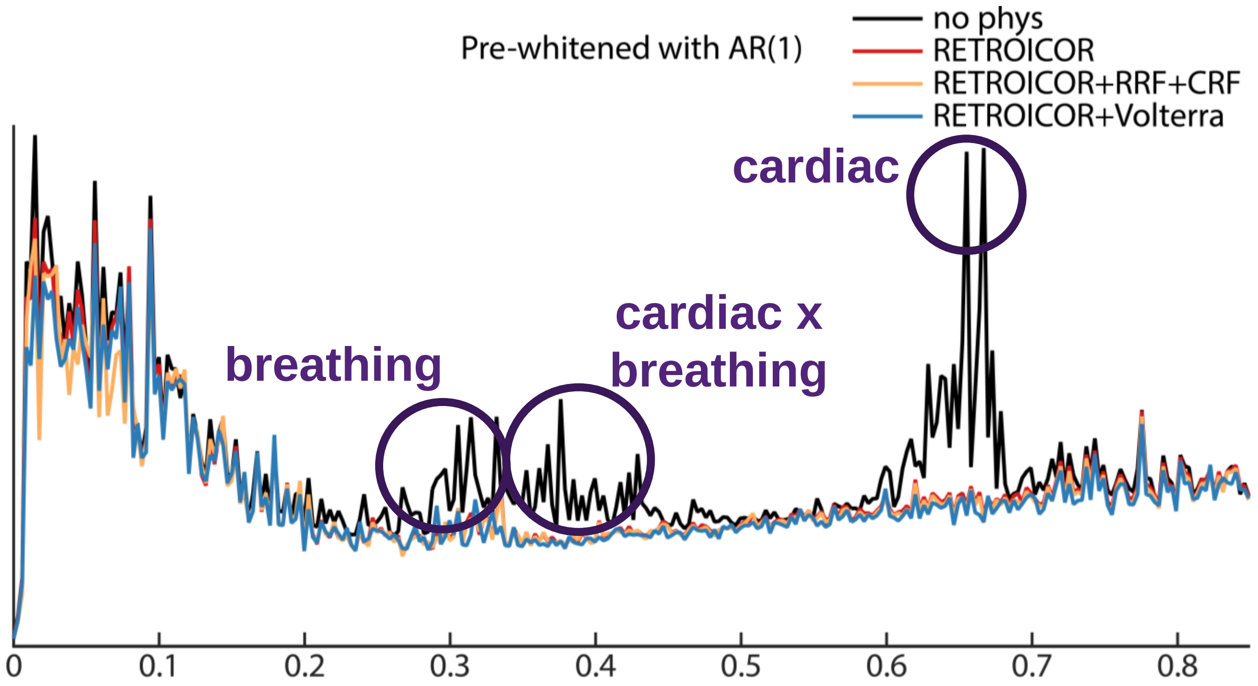

Bollmann et al., 2018, NI

Better pre-whitening performance

- AFNI: ARMA(1,1)
- SPM: FAST

On the Analysis of Rapidly Sampled fMRI Data[1]

Task

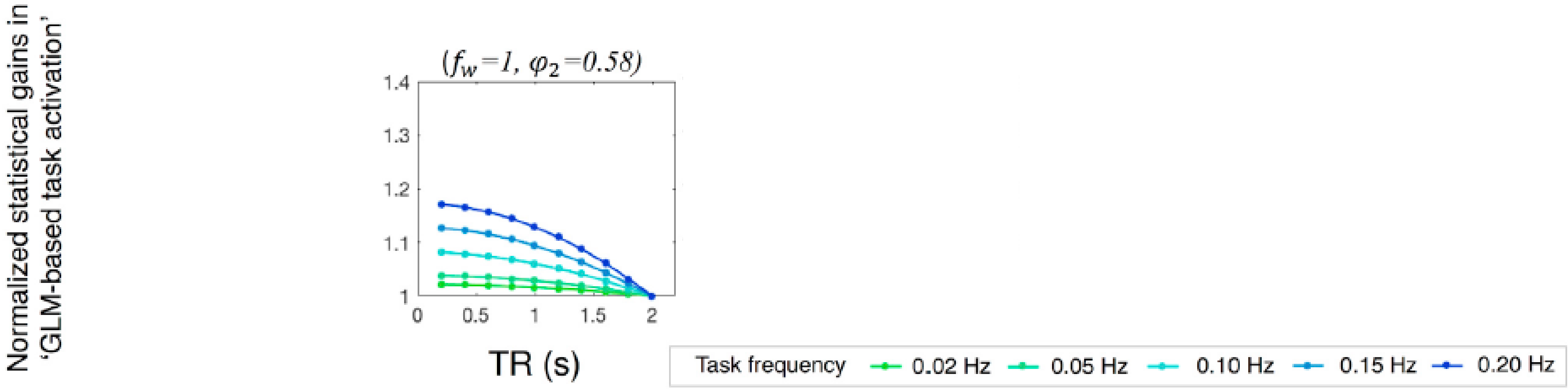

More statistical gains for

- Faster task

[1]Chen et al., 2019, NI

On the Analysis of Rapidly Sampled fMRI Data[1]

Task

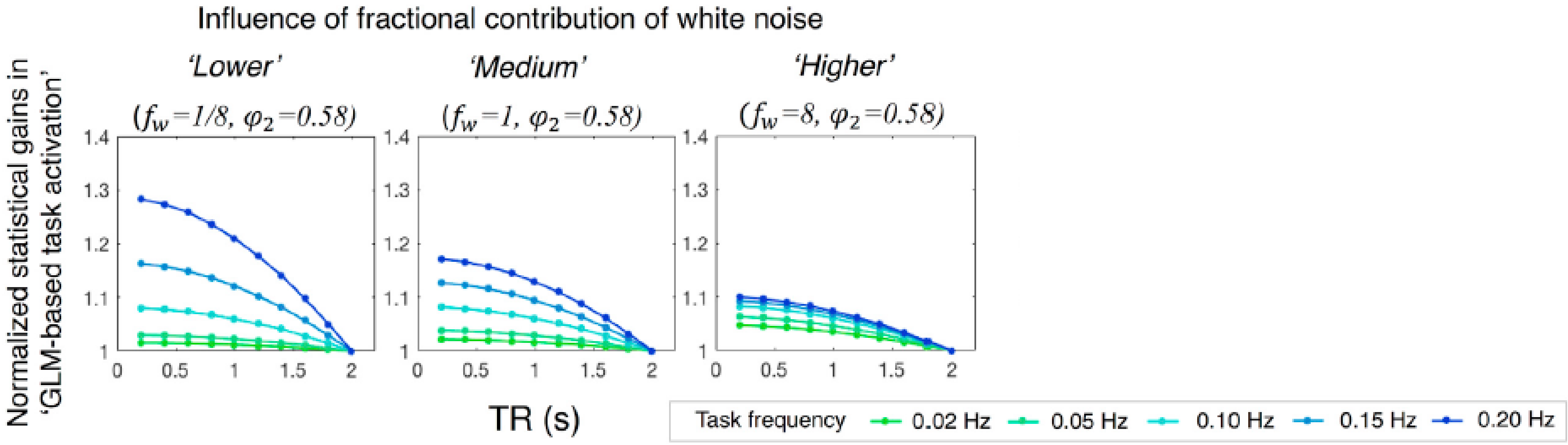

More statistical gains for

- Faster task
- Less white noise

[1]Chen et al., 2019, NI

On the Analysis of Rapidly Sampled fMRI Data[1]

Task

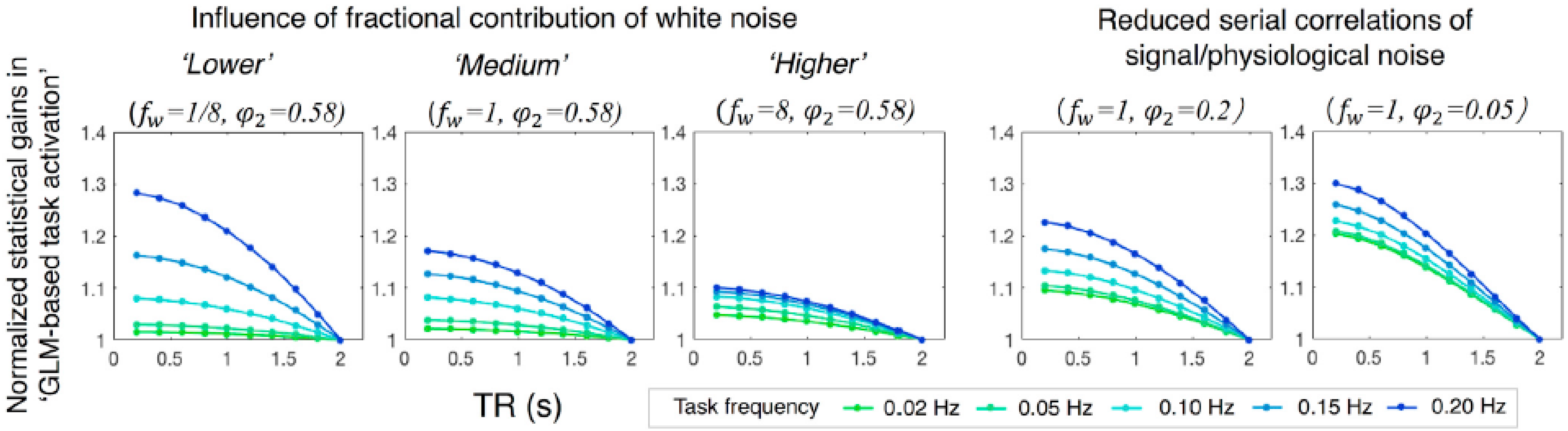

More statistical gains for

- Faster task
- Less white noise
- Less serial correlations

[1]Chen et al., 2019, NI

Fast fMRI

Analysis: Dynamic stimuli

Fast fMRI Can Detect Oscillatory Neural Activity in Humans[1]

resolution 2.5 mm iso **TR = 246 ms**

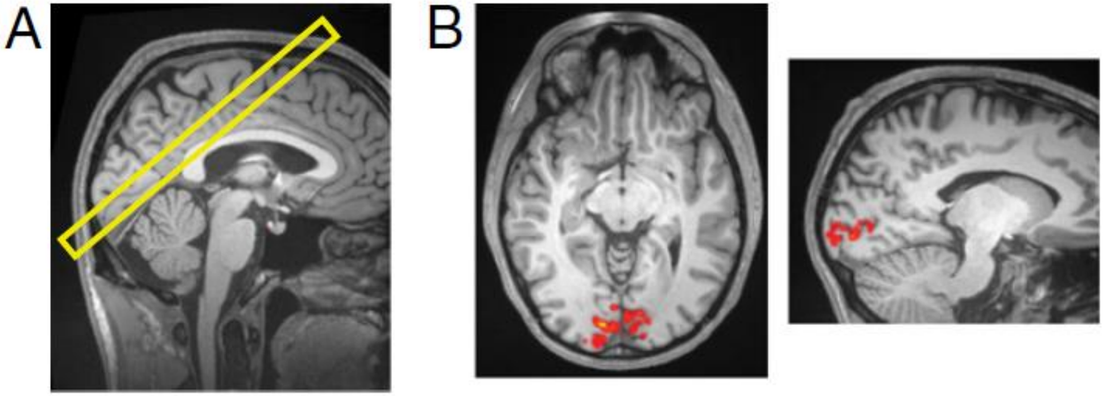

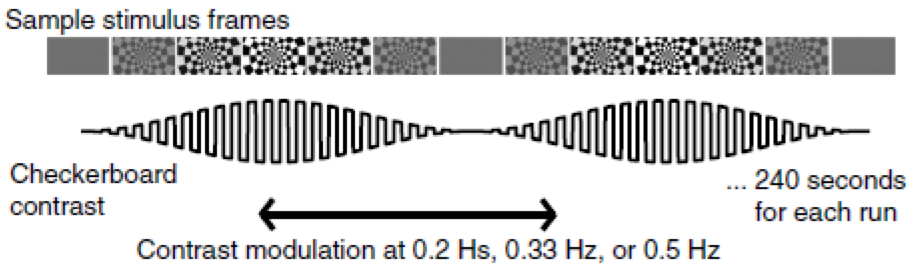

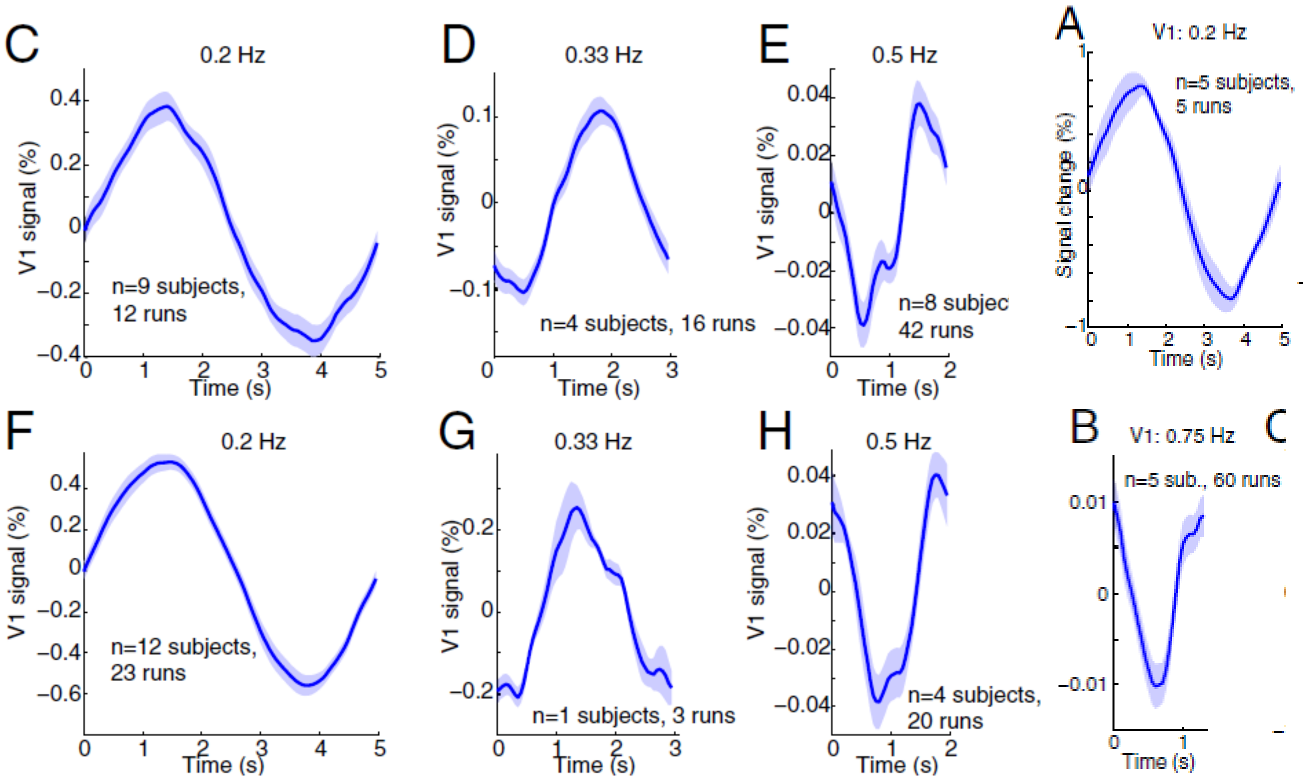

3T **7T**

[1]Lewis et al., 2016, PNAS

High-resolution fMRI

Acquisition: 3D-EPI

3D Echo-Planar Imaging (3D EPI)[1,2]

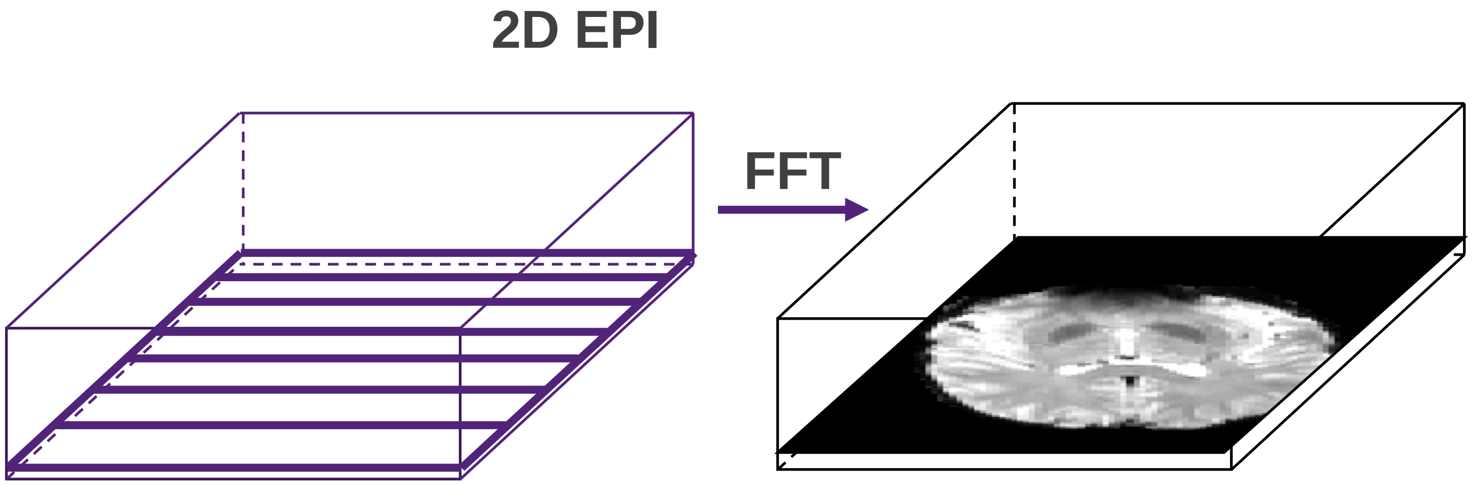

[1]Mansfield, J. Phys. C: Solid State Phys, 1977; [2]Poser et al., NI, 2010

3D Echo-Planar Imaging (3D EPI)[1,2]

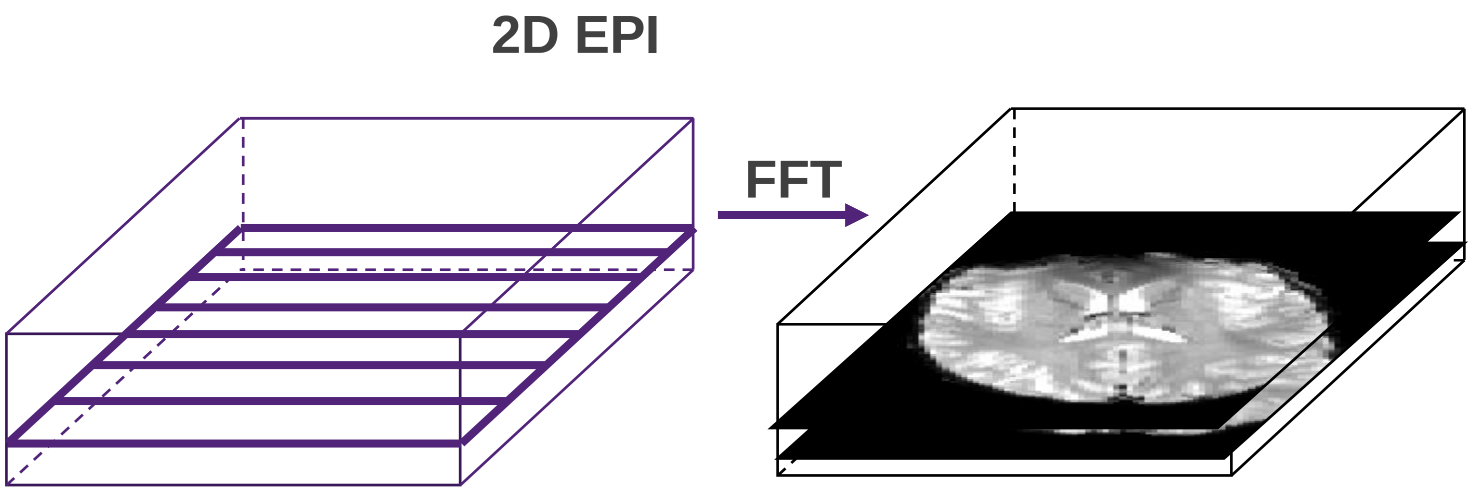

[1]Mansfield, J. Phys. C: Solid State Phys, 1977; [2]Poser et al., NI, 2010

3D Echo-Planar Imaging (3D EPI)[1,2]

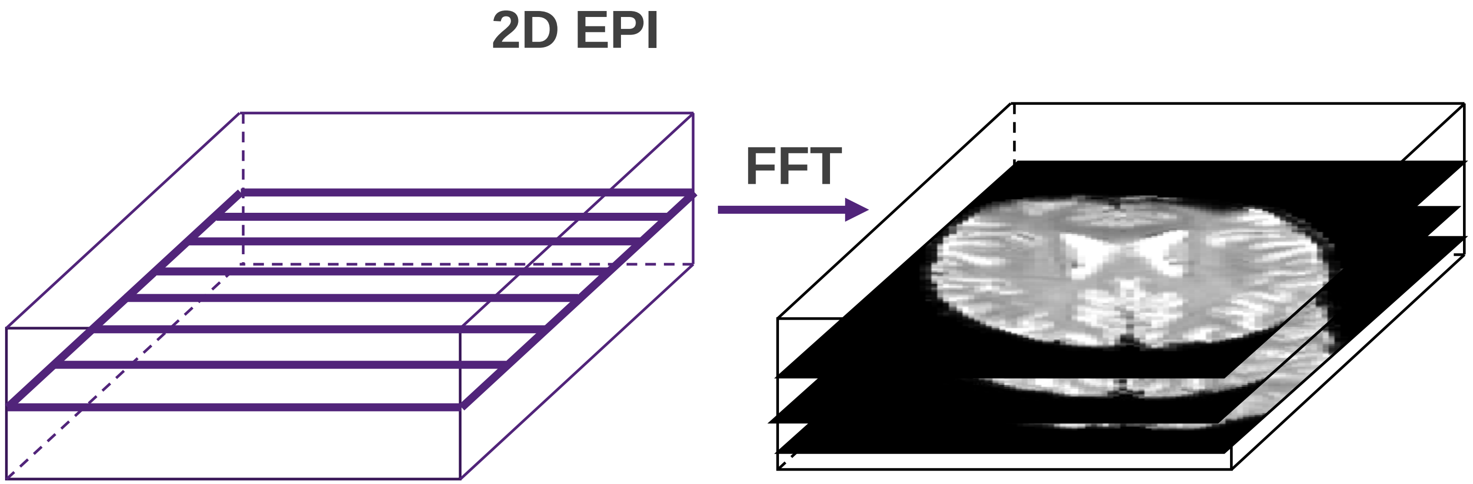

[1]Mansfield, J. Phys. C: Solid State Phys, 1977; [2]Poser et al., NI, 2010

3D Echo-Planar Imaging (3D EPI)[1,2]

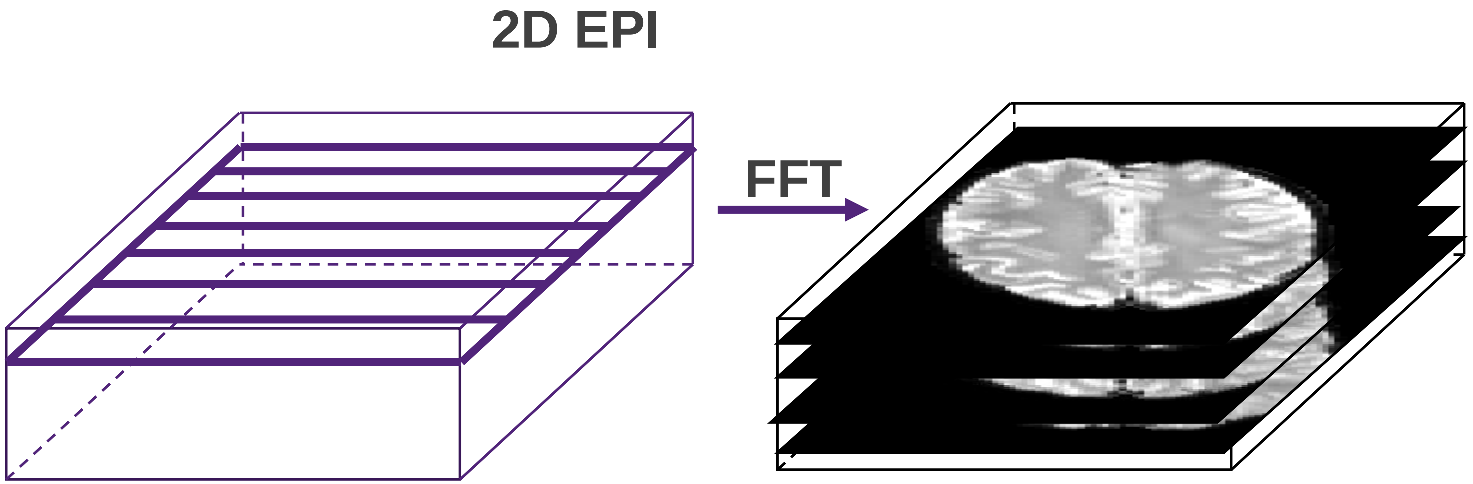

[1]Mansfield, J. Phys. C: Solid State Phys, 1977; [2]Poser et al., NI, 2010

3D Echo-Planar Imaging (3D EPI)[1,2]

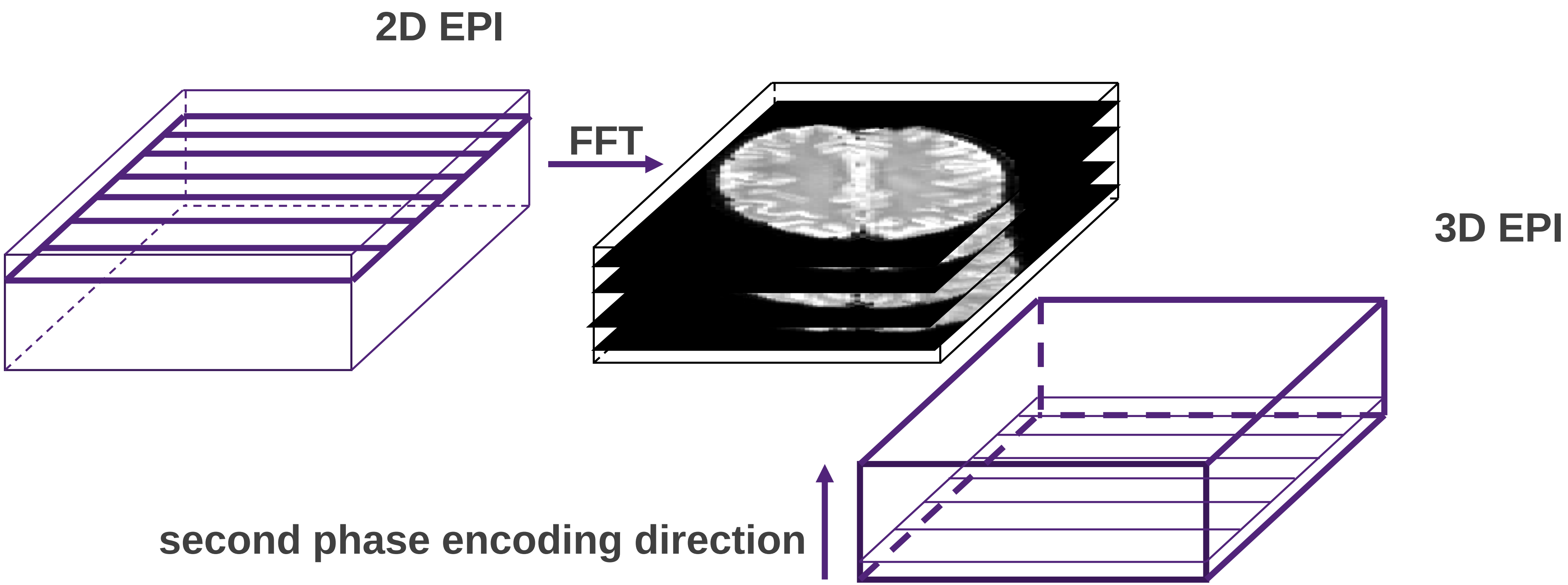

[1]Mansfield, J. Phys. C: Solid State Phys, 1977; [2]Poser et al., NI, 2010

3D Echo-Planar Imaging (3D EPI)[1,2]

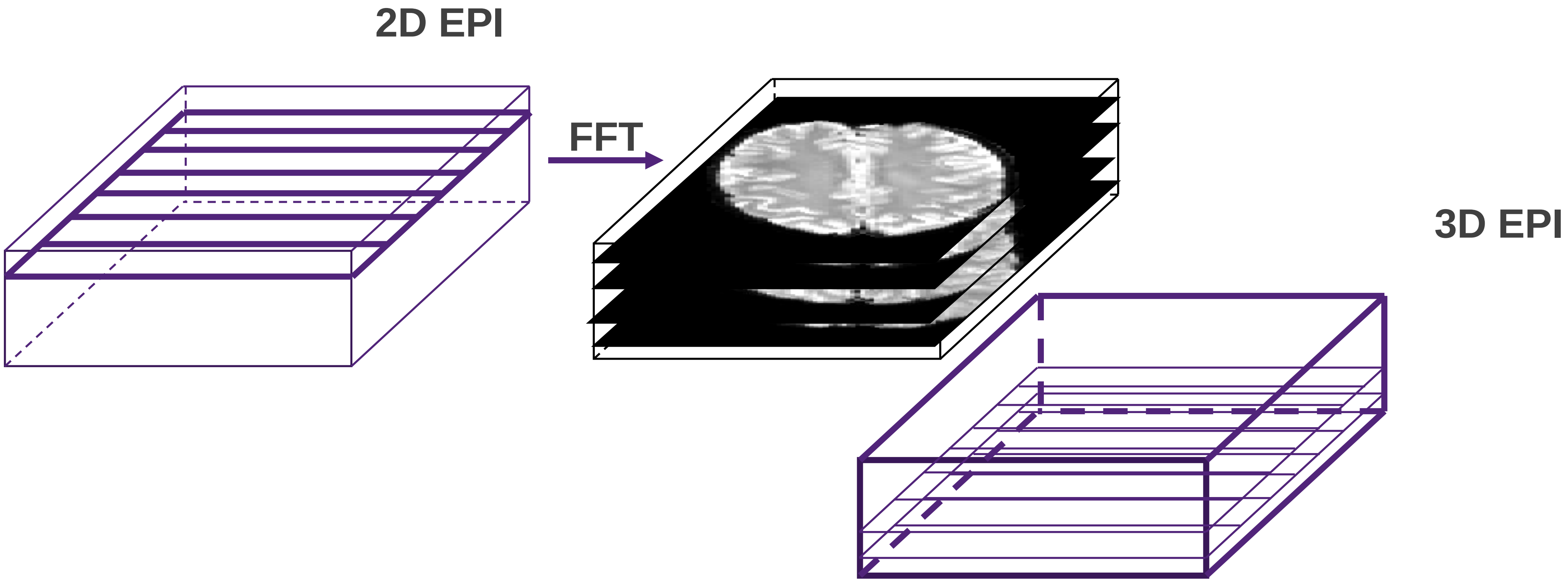

[1]Mansfield, J. Phys. C: Solid State Phys, 1977; [2]Poser et al., NI, 2010

3D Echo-Planar Imaging (3D EPI)[1,2]

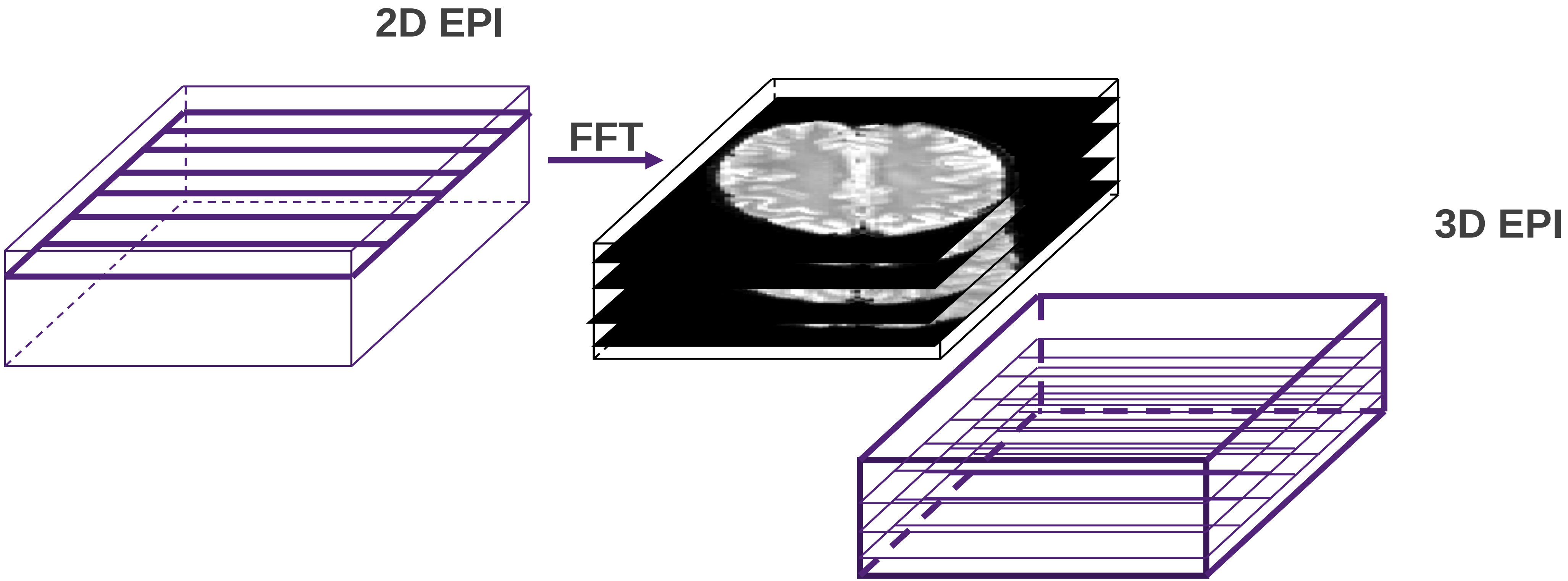

[1]Mansfield, J. Phys. C: Solid State Phys, 1977; [2]Poser et al., NI, 2010

3D Echo-Planar Imaging (3D EPI)[1,2]

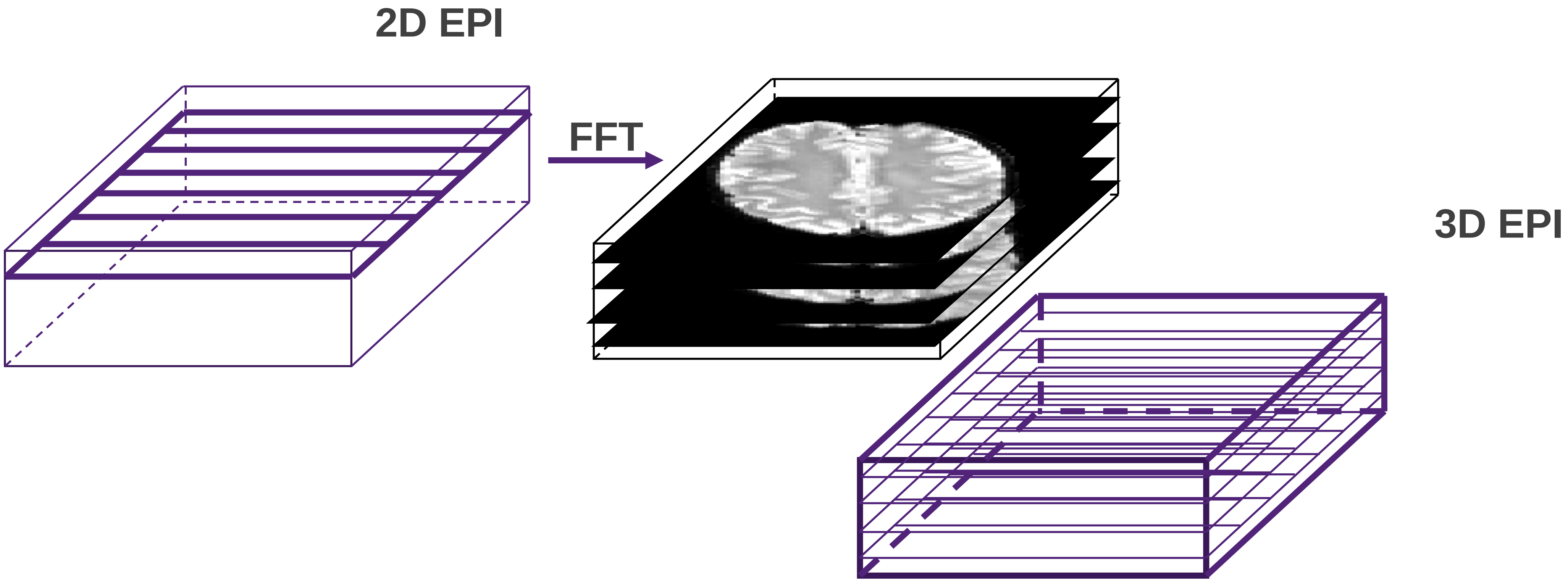

[1]Mansfield, J. Phys. C: Solid State Phys, 1977; [2]Poser et al., NI, 2010

3D Echo-Planar Imaging (3D EPI)[1,2]

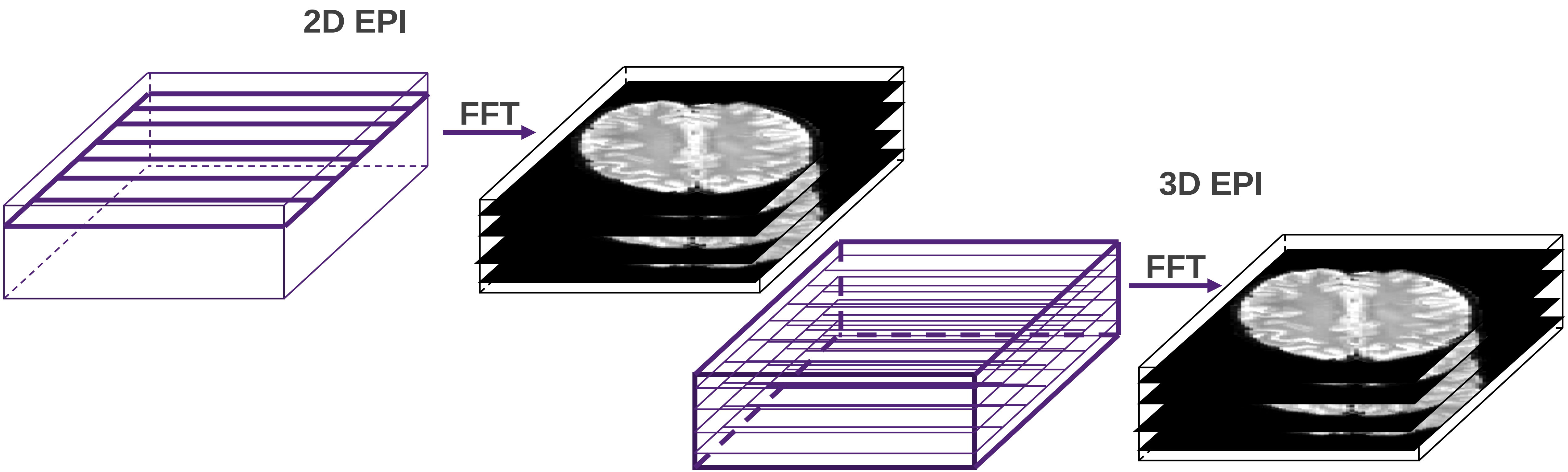

[1]Mansfield, J. Phys. C: Solid State Phys, 1977; [2]Poser et al., NI, 2010

High-resolution fMRI acquisition

- high-resolution fMRI → sub-millimetre resolution
- majority of studies utilize a 3D EPI acquisition
  - higher temporal SNR than 2D at sub-millimetre resolution[1]

Huber et al., NI, 2020

[1]Lutti et al., MRM, 2013; Huber et al., NI, 2018

3D Echo-Planar Imaging (3D EPI)[1,2]

- higher temporal SNR than 2D at sub-millimetre resolution[3,4]

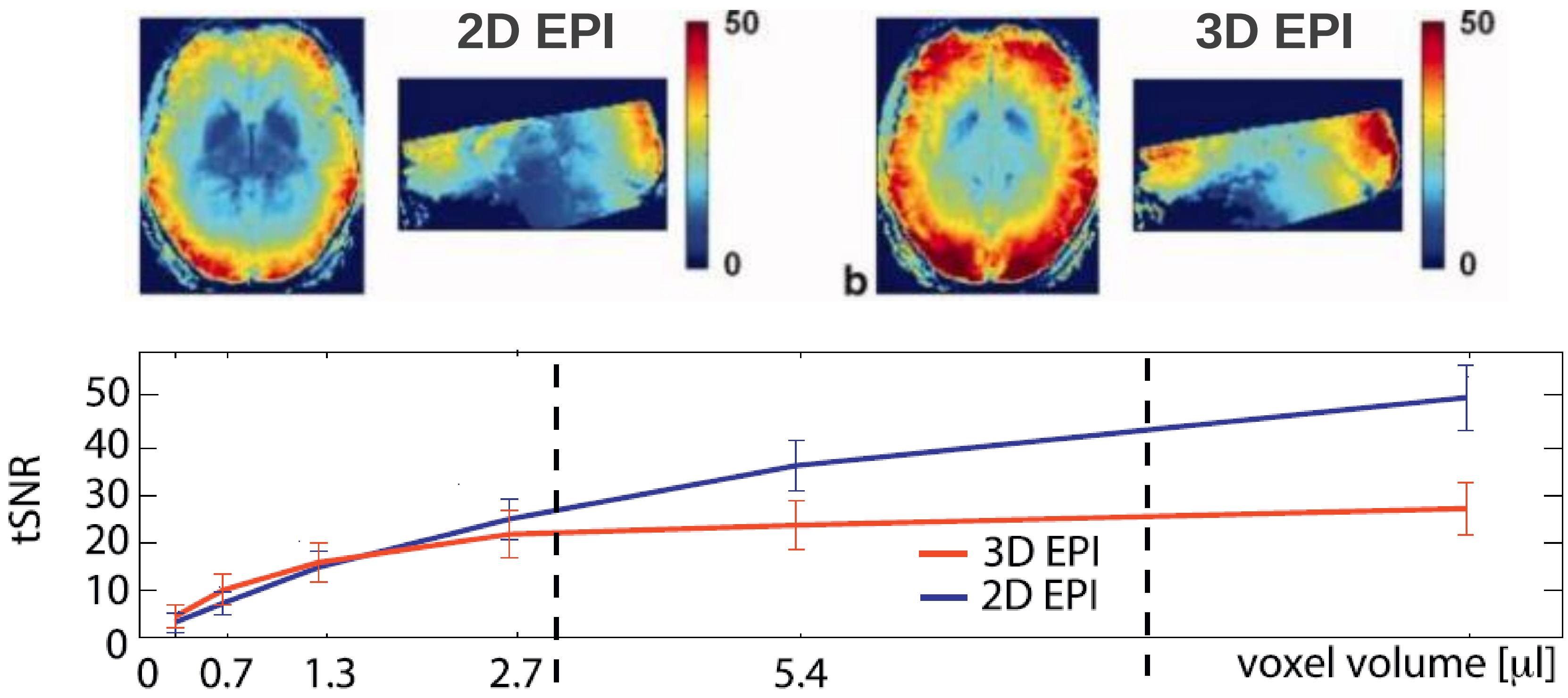

[1]Mansfield, J. Phys. C: Solid State Phys, 1977; [2]Poser et al., NI, 2010; [3]Lutti et al., MRM, 2013; [4]Huber et al., NI, 2018

High-resolution fMRI acquisition

- high-resolution fMRI → sub-millimetre resolution
- majority of studies utilize a 3D EPI acquisition
  - higher temporal SNR than 2D at sub-millimetre resolution[1]
  - low SAR/better slice profile
- current parameter 'optimum'
  - 0.7 – 1 mm resolution
  - 25 – 35 ms TE
  - 2 – 3 s TR (partial coverage)
  - R = 4
  - 6/8 – no PF
- current limitations
  - image fidelity (blurring & B_0)
  - resolution/TE

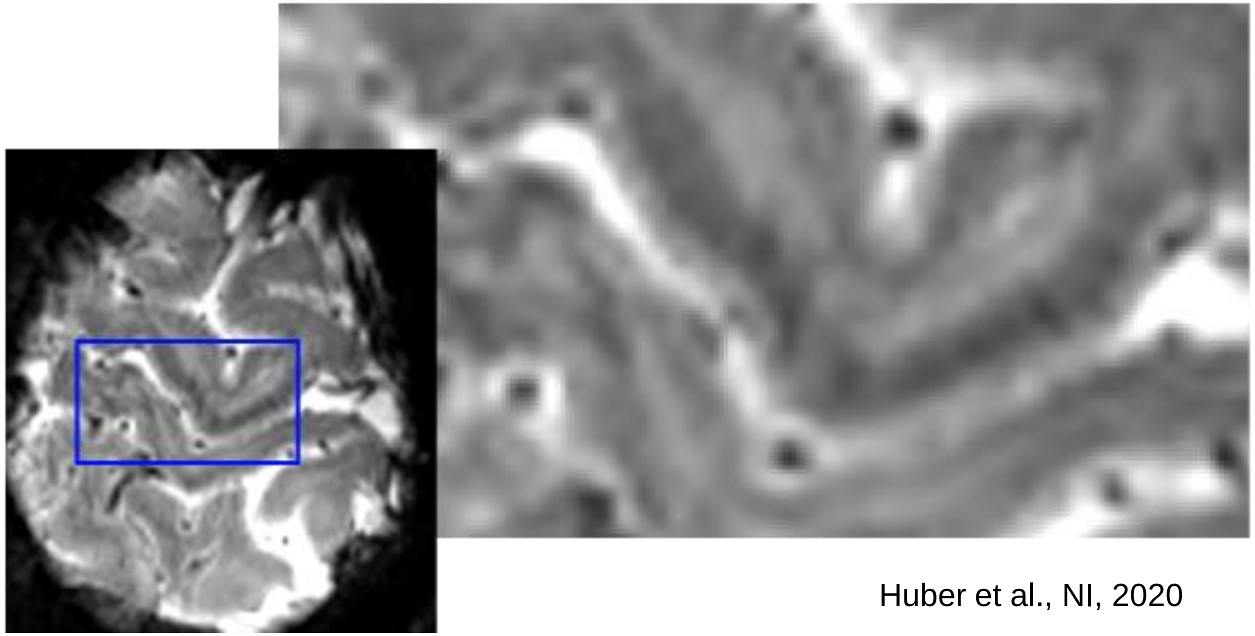

Huber et al., NI, 2020

[1]Lutti et al., MRM, 2013; Huber et al., NI, 2018

High-resolution fMRI

Cortical architecture

Cortical Architecture

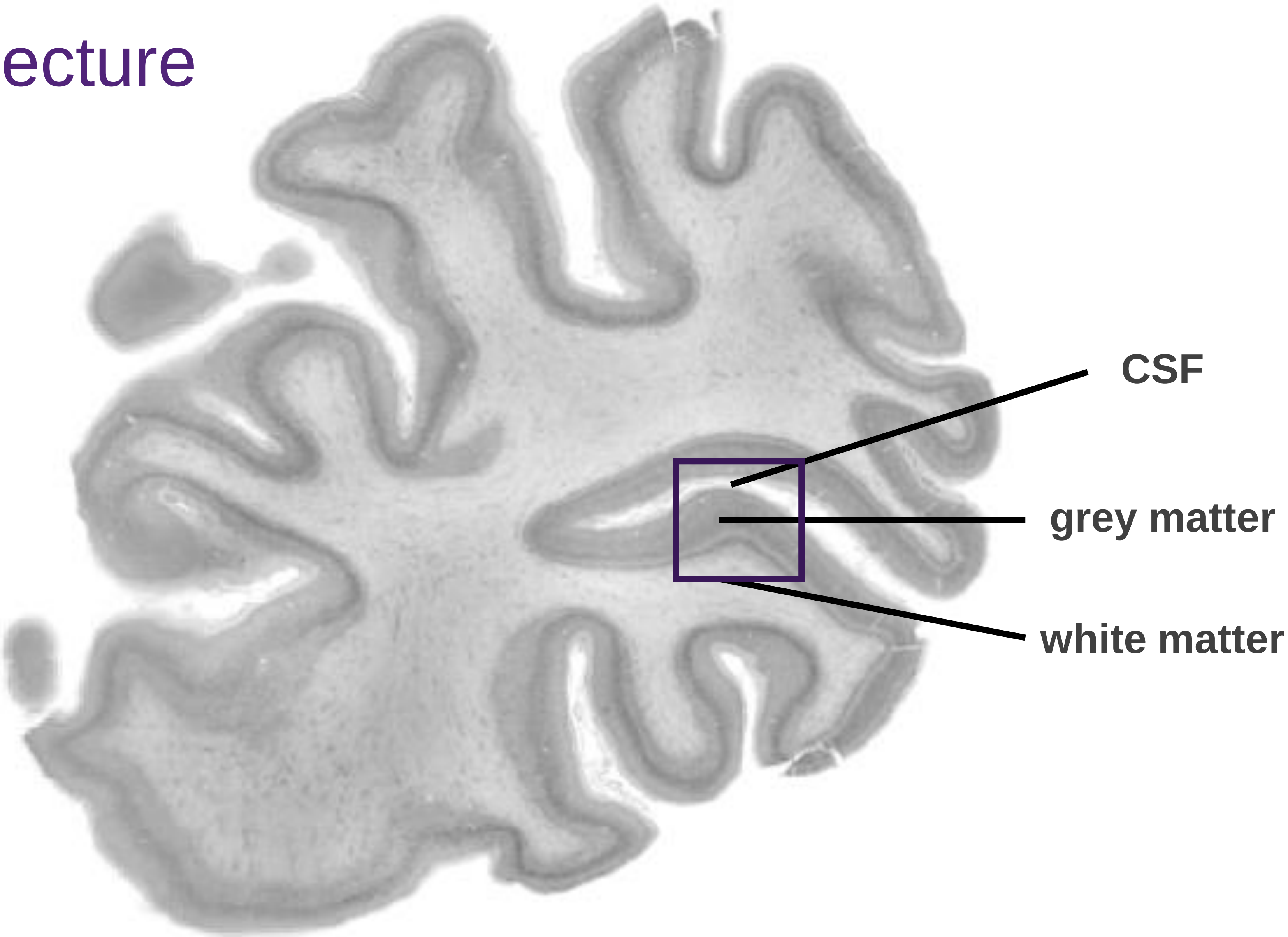

Amunts et al., Science, 2013

Coordinate system for high-resolution fMRI

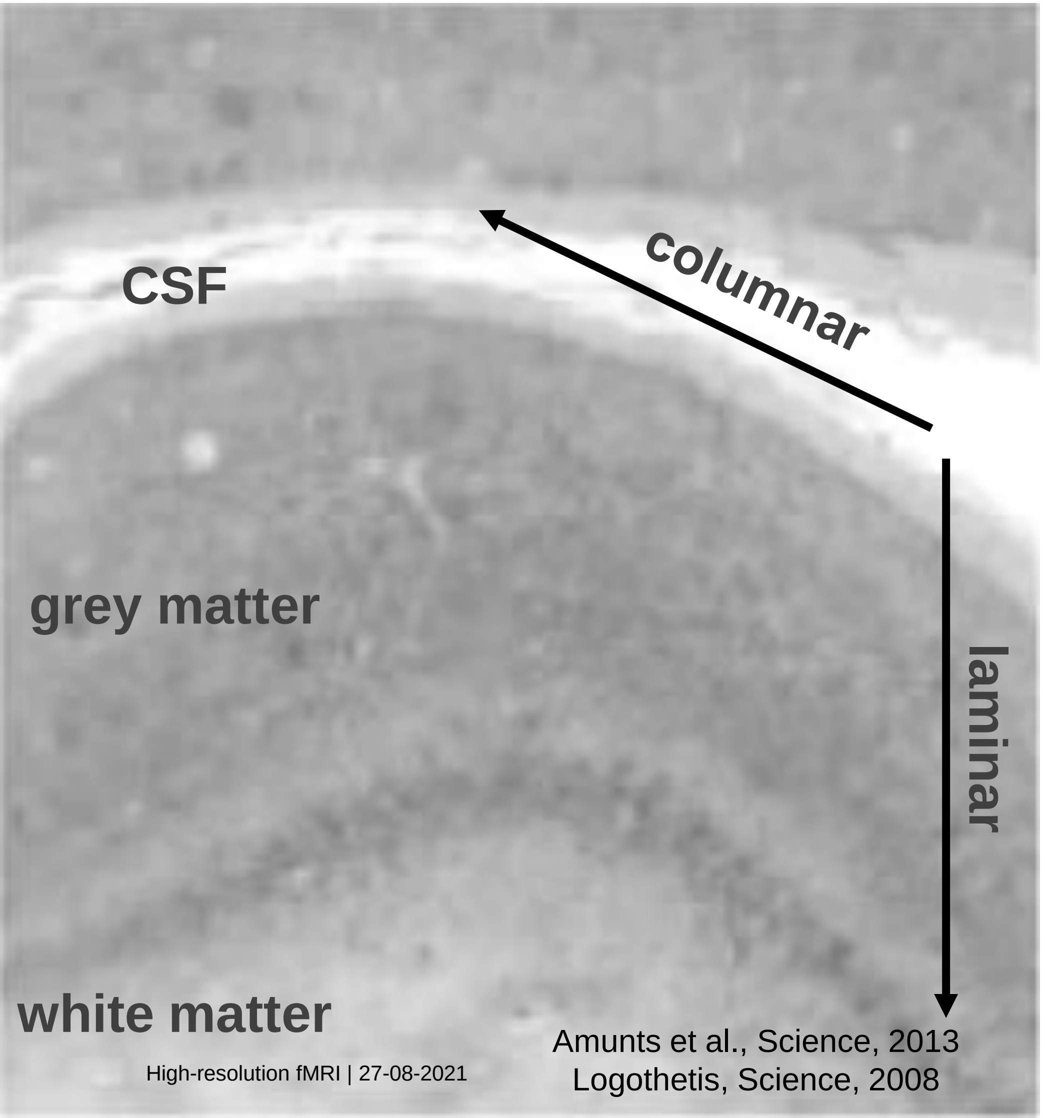

Amunts et al., Science, 2013
Logothetis, Science, 2008

- 2 main partitioning axes of the cortex[1]
  - perpendicular to the surface → laminar (= depth-dependent)[2]
  - parallel to the surface → columnar (= topographic)[3]

[1]Harris and Mrsic-Flogel, Nature, 2013; Shamir and Assaf, medRxiv, 2020
[2]Barth and Norris, NMR Biomed, 2007; Polimeni et al., NI, 2010; Olman et al., PlosOne, 2012; Huber et al., Neuron, 2017
[3]Engel et al., Nature, 1994; Sereno et al., Science, 1995; Wandell et al., Neuron, 2007; Silver and Kastner, Trends in Cogn Sciences, 2009; Sanchez-Panchuelo et al., J Neurosci, 2012; Besle et al., J Neurphysiology, 2013; Puckett et al., Neuroimage, 2017; Wessinger et al., HBM, 1997; Bilecen et al., Hearing Research. 1998; Talavage et al., J Neurphysiology, 2004; Ahveninen et al., NI, 2016

High-resolution fMRI

Analysis: Topographic analysis

Ocular dominance columns

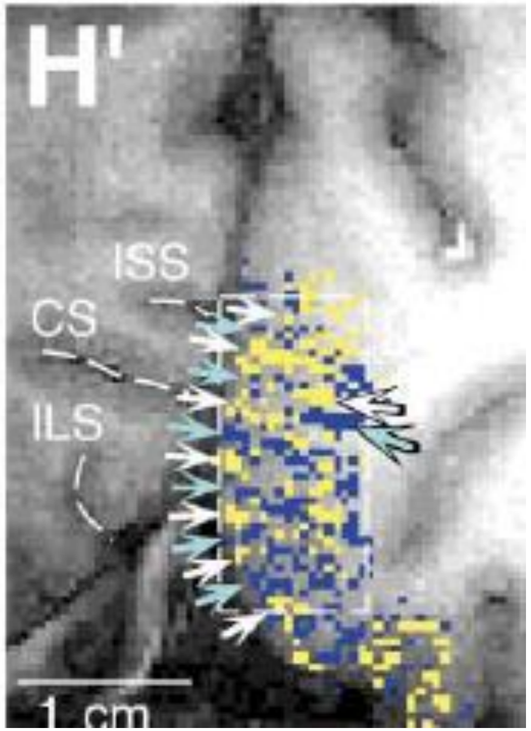

Cheng et al., Neuron, 2001

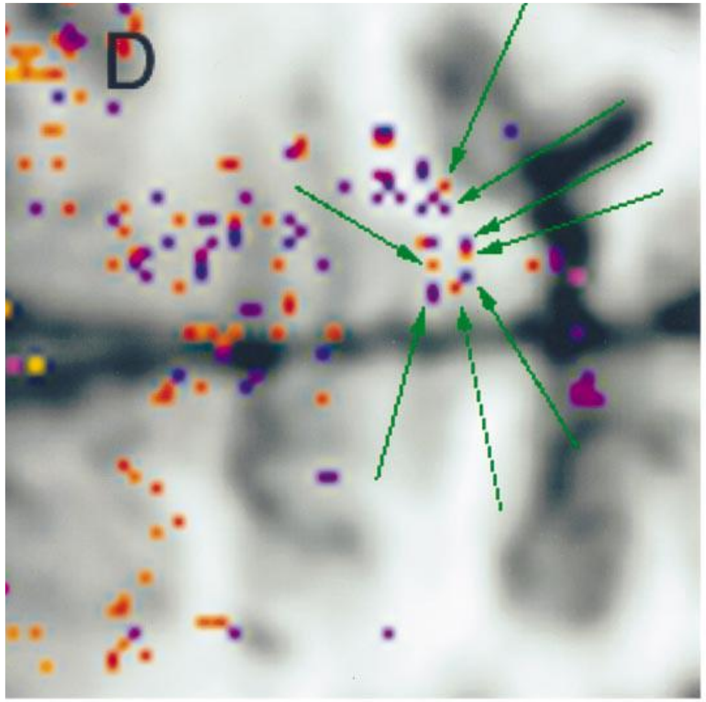

Menon et al., J Neurophysiol, 1997

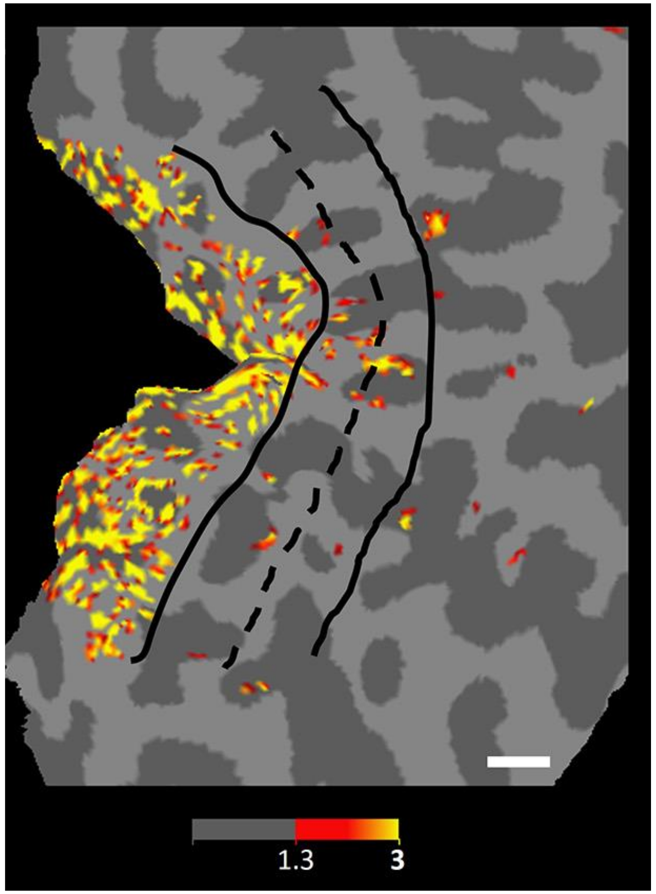

Nasr et al., J Neurosci, 2016

Attention in somatosensory cortex

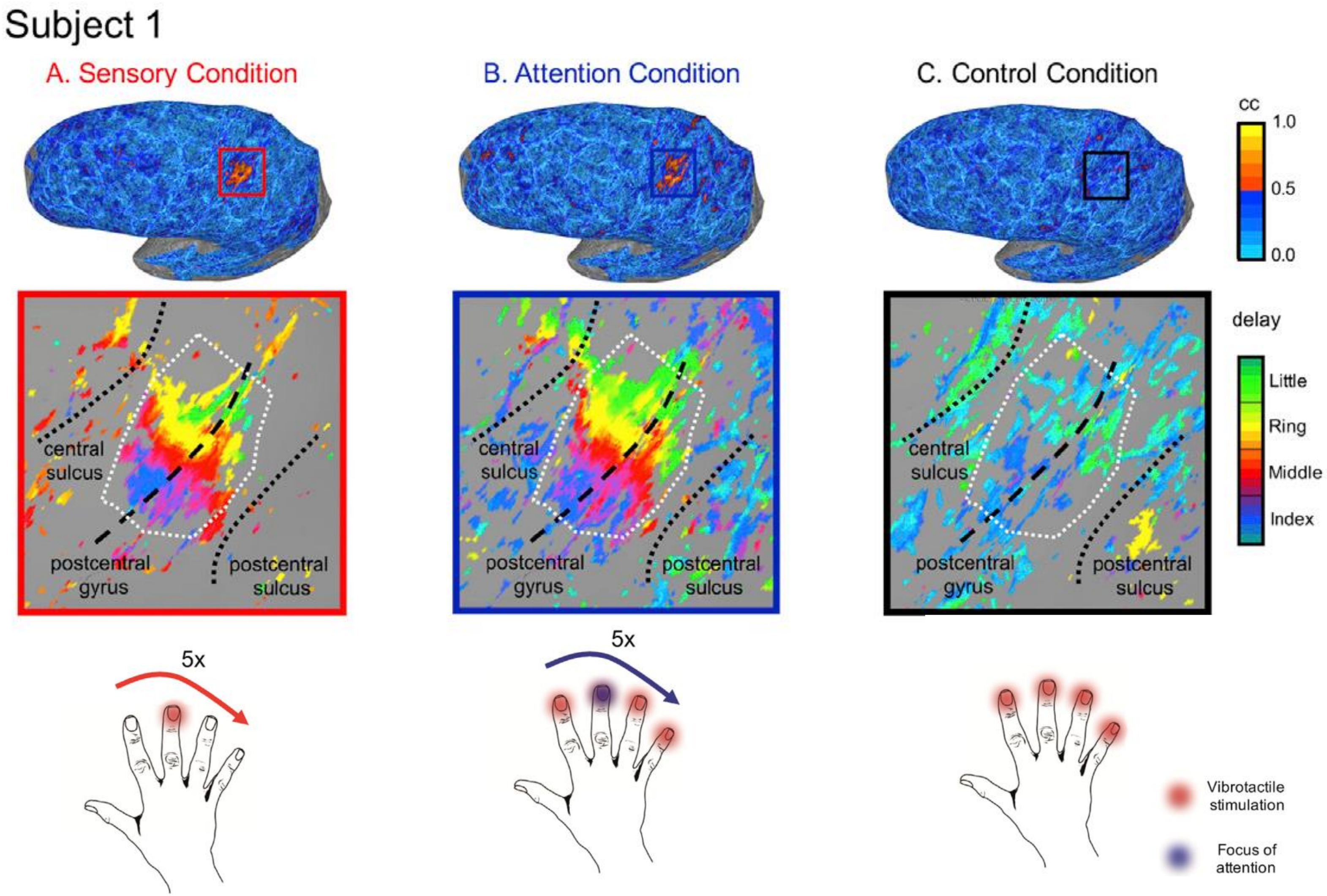

Puckett et al., NI, 2017

High-resolution fMRI

Analysis: Depth-dependent analysis

The University of Queensland
Australia

THE UNIVERSITY OF QUEENSLAND AUSTRALIA

Coordinate system for high-resolution fMRI

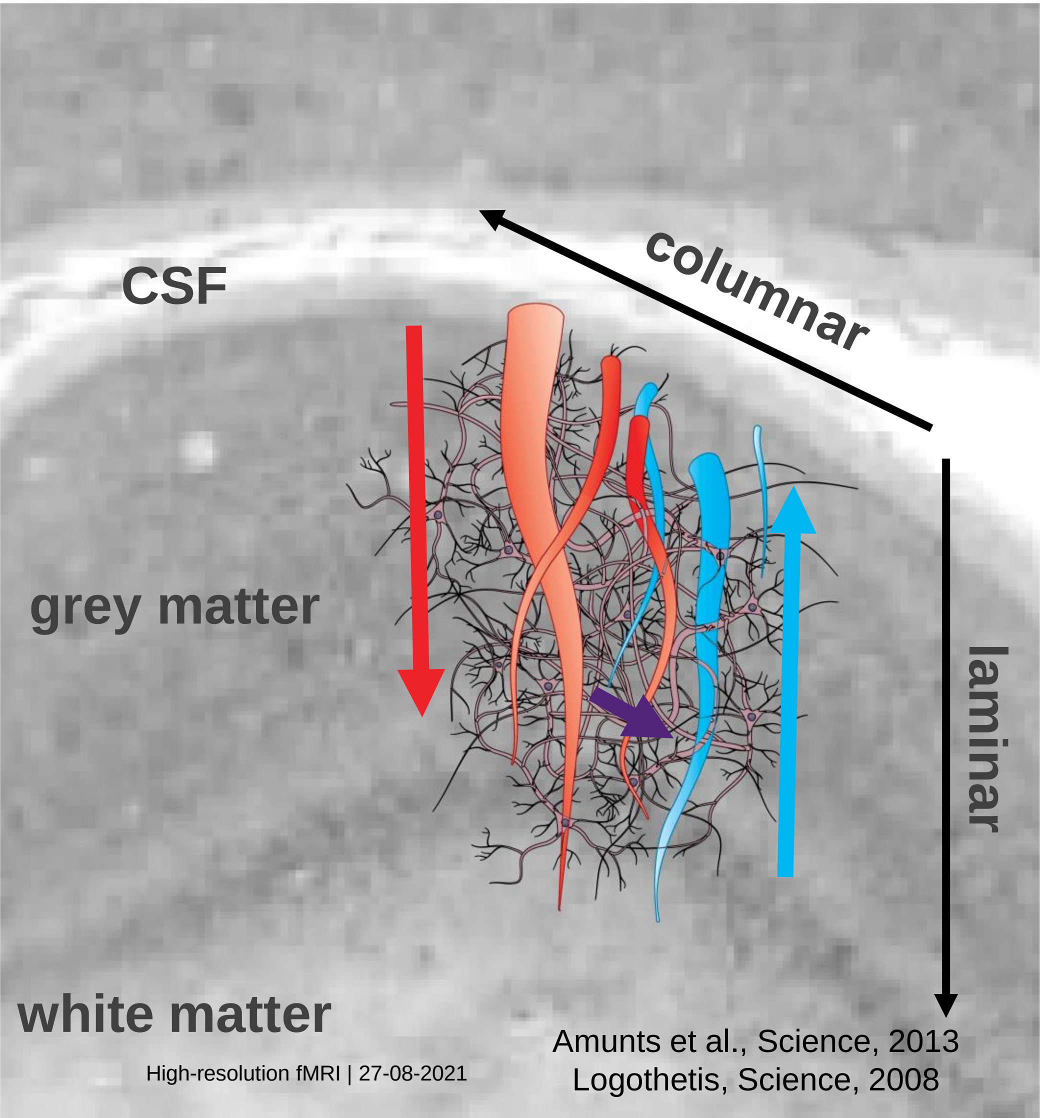

Amunts et al., Science, 2013
Logothetis, Science, 2008

- 2 main partitioning axes of the cortex[1]
  - perpendicular to the surface → laminar (= depth-dependent)[2]
  - parallel to the surface → columnar (= topographic)[3]

[1]Harris and Mrsic-Flogel, Nature, 2013; Shamir and Assaf, medRxiv, 2020
[2]Barth and Norris, NMR Biomed, 2007; Polimeni et al., NI, 2010; Olman et al., PlosOne, 2012; Huber et al., Neuron, 2017
[3]Engel et al., Nature, 1994; Sereno et al., Science, 1995; Wandell et al., Neuron, 2007; Silver and Kastner, Trends in Cogn Sciences, 2009; Sanchez-Panchuelo et al., J Neurosci, 2012; Besle et al., J Neurphysiology, 2013; Puckett et al., Neuroimage, 2017; Wessinger et al., HBM, 1997; Bilecen et al., Hearing Research. 1998; Talavage et al., J Neurphysiology, 2004; Ahveninen et al., NI, 2016

An increase in % BOLD signal change is commonly observed across cortical depths

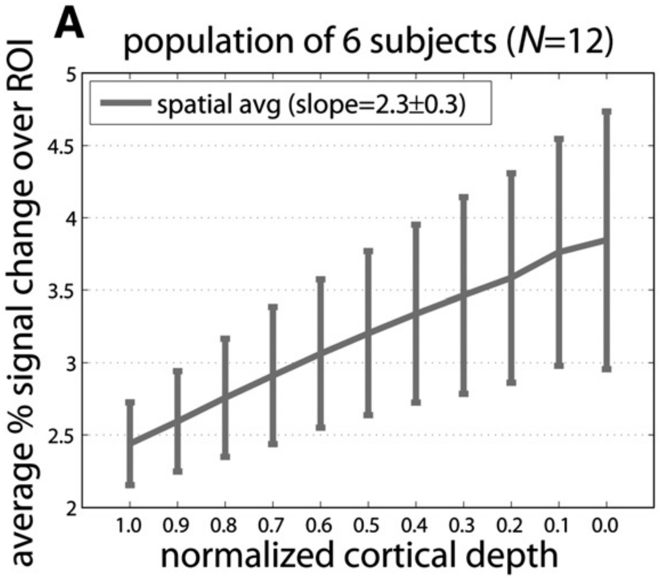

Polimeni et al., NI, 2010

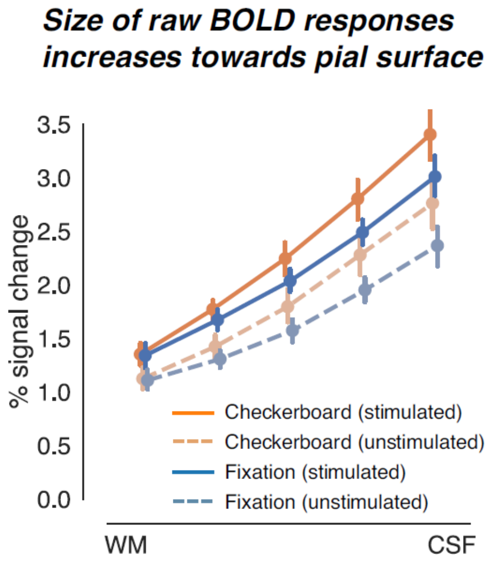

de Hollander et al., NI, 2021

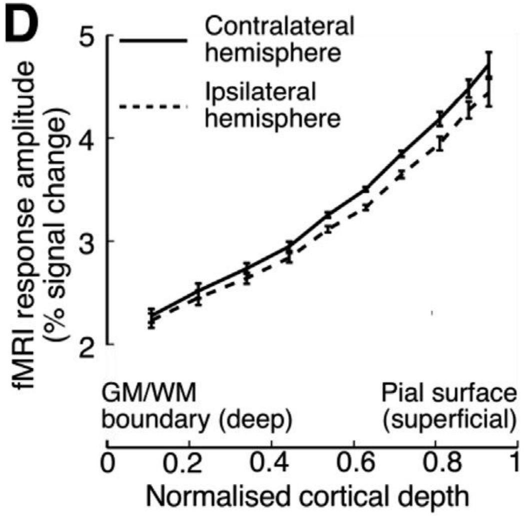

Klein et al., NI, 2018

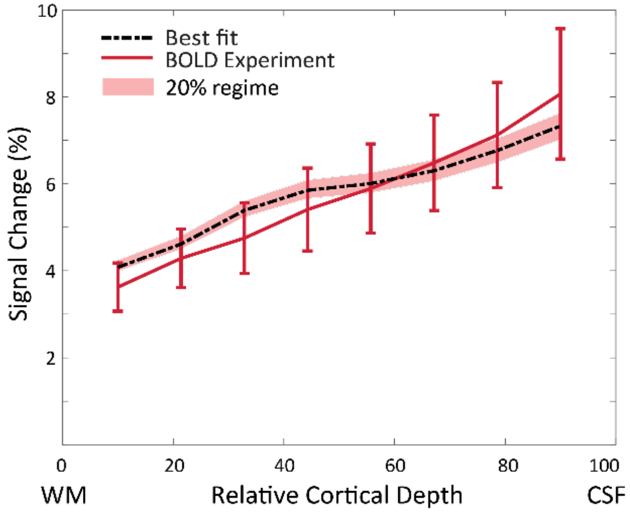

Akbari et al., biorxiv, 2021

Sources of the pial bias

Pial veins

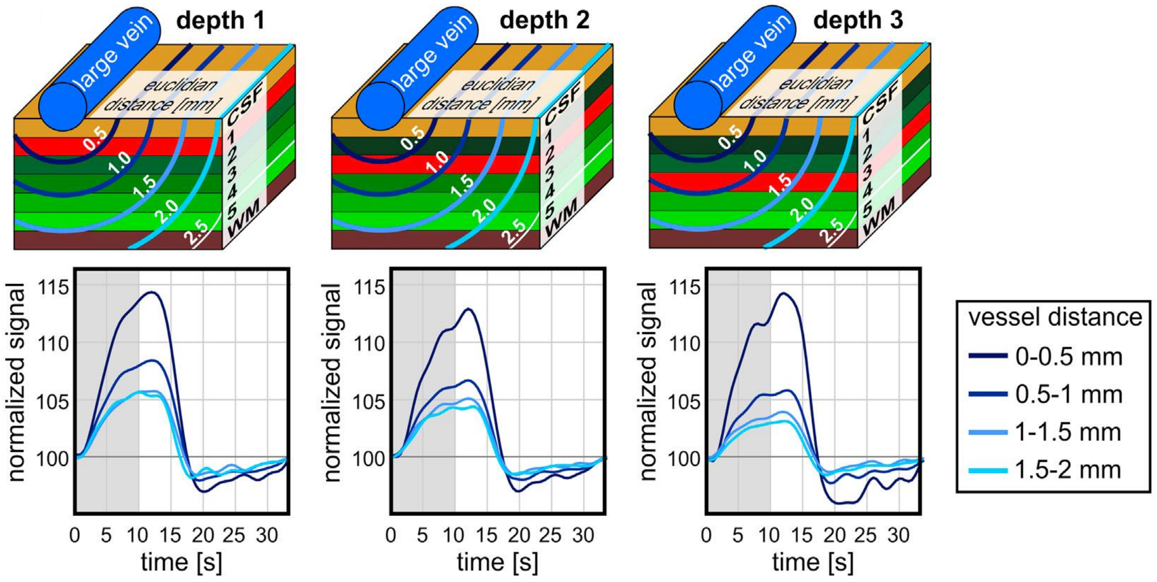

Bause et al., NI, 2020

Or intracortical veins?

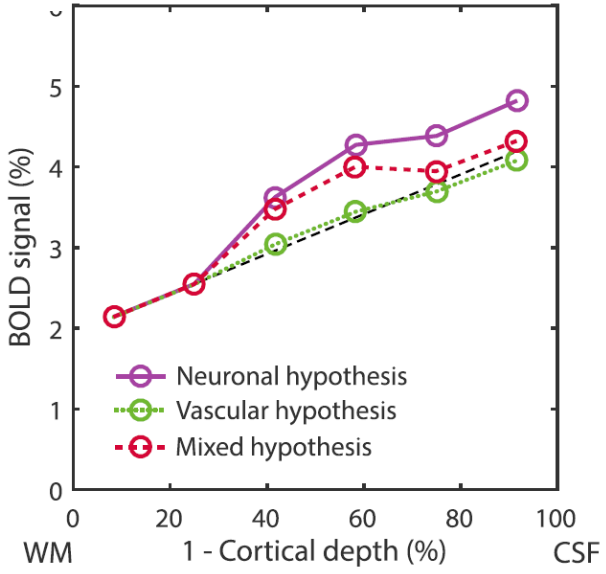

Havlicek and Uludağ, NI, 2020

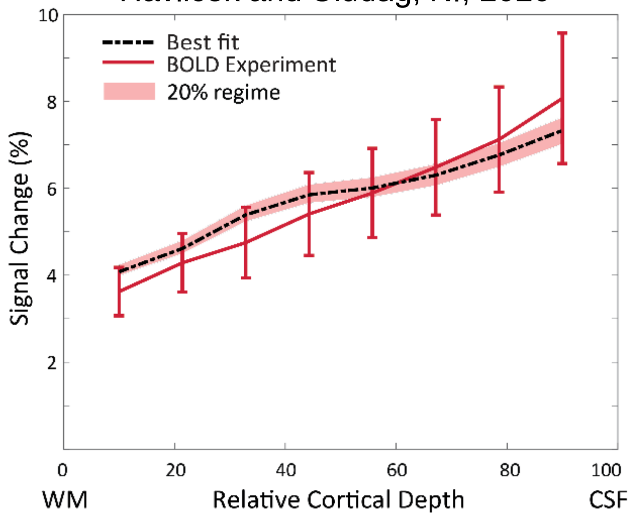

Akbari et al., biorxiv, 2021

Addressing the pial bias through

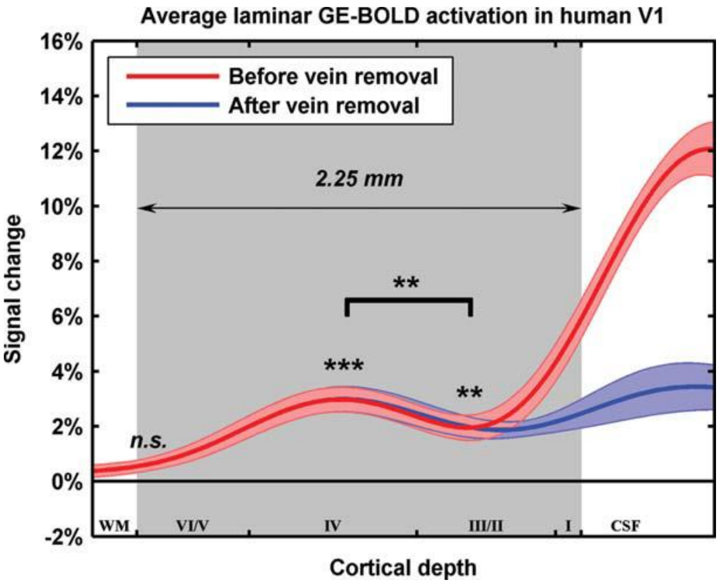

Koopmans et al., HBM, 2010

FLASH imaging and vein removal

Laminar deconvolution estimates signal contribution of different cortical depths

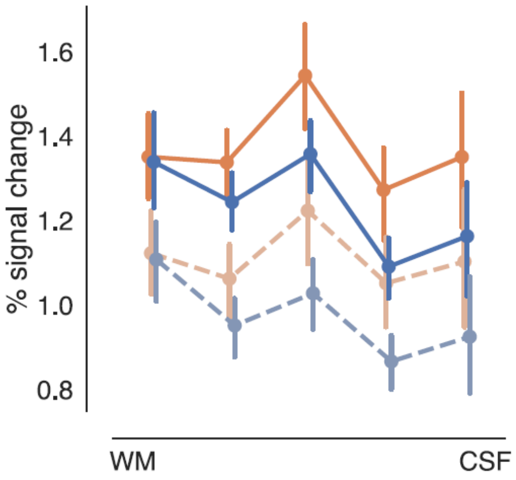

de Hollander et al., NI, 2021

deconvolution

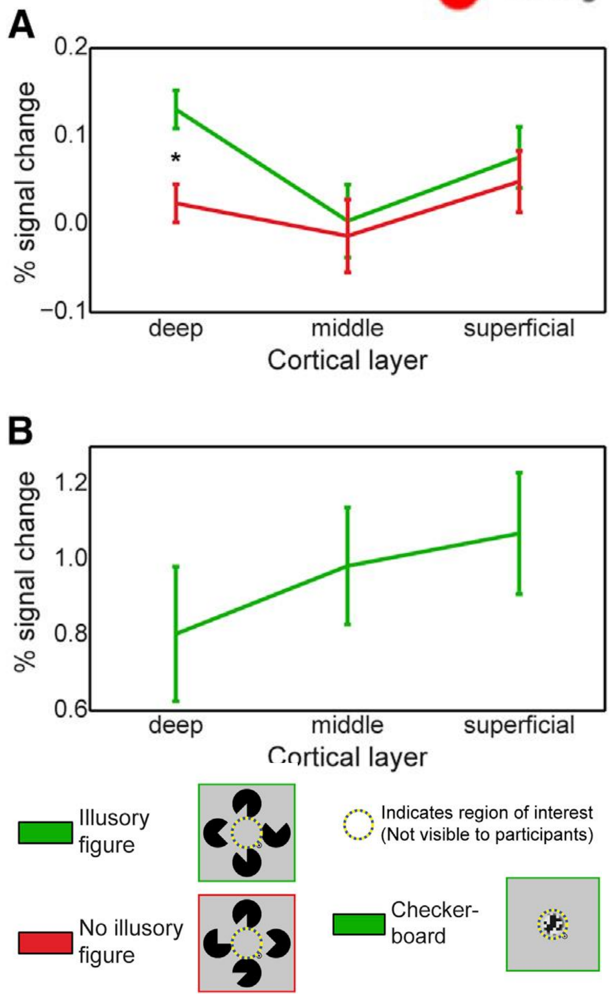

Kok et al., Current Biology, 2016

experimental design

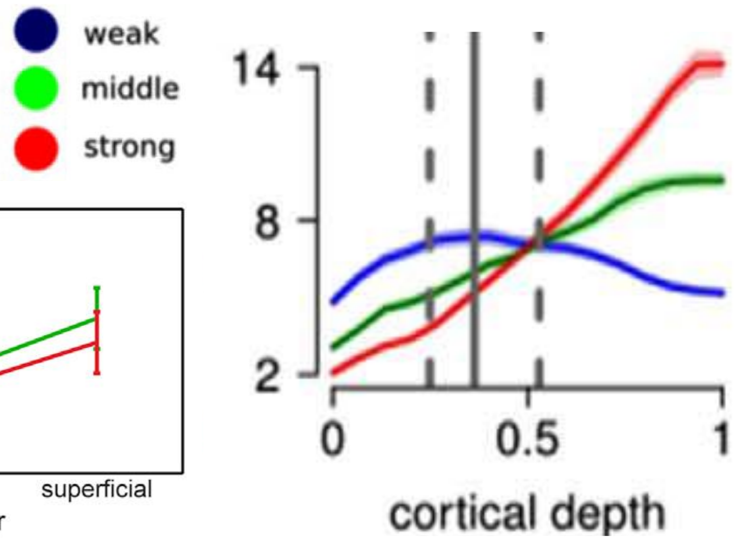

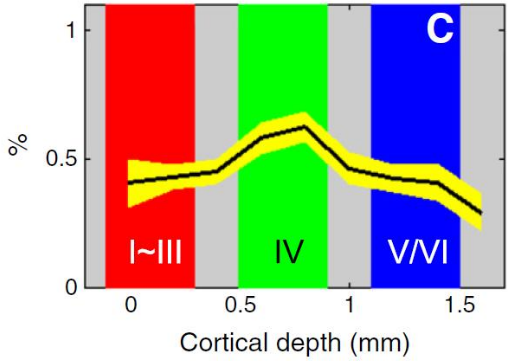

Fracasso et al., NI, 2018
Chen et al., NI, 2013

voxel sorting

Beyond vasculature: acquisition and analysis challenges[1,2,3]

Acquisition

- Distortions due to B_0 inhomogeneities
- T_2^* blurring
- Partial Fourier

Analysis

- Registration of structural and functional images
- GM/WM and GM/CSF boundary definition
- Definition of ‘depth’

Polimeni et al., NI, 2018; Weldon and Olman, Phil. Trans. R. Soc. B, 2021; https://layerfmri.com/

Pushing the limits of fMRI at ultra-high field

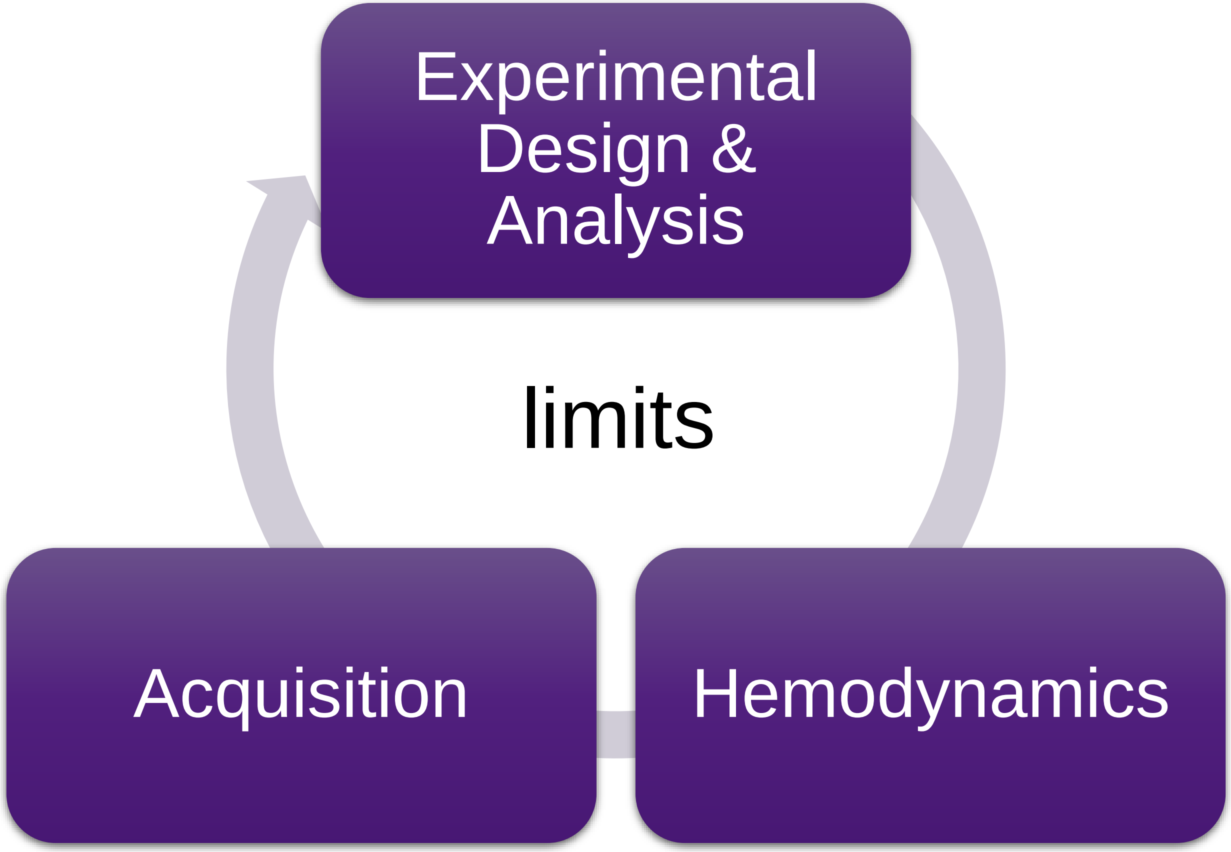

3D-EPI Siemens WIP 1043A&B

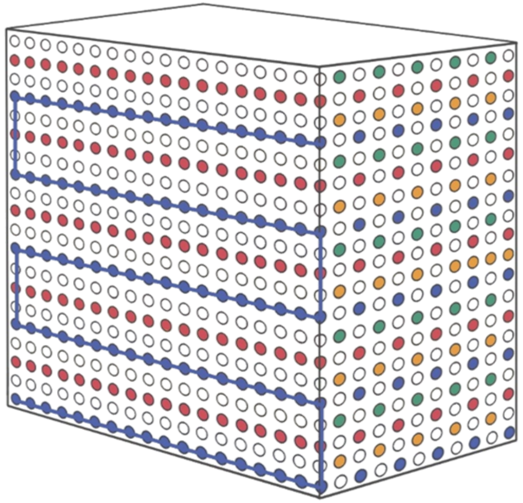

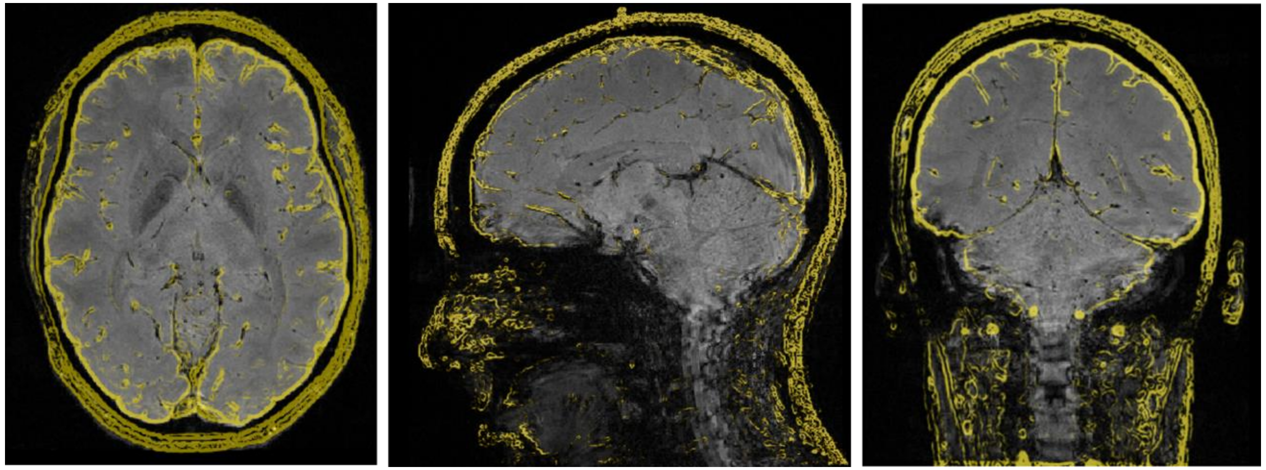

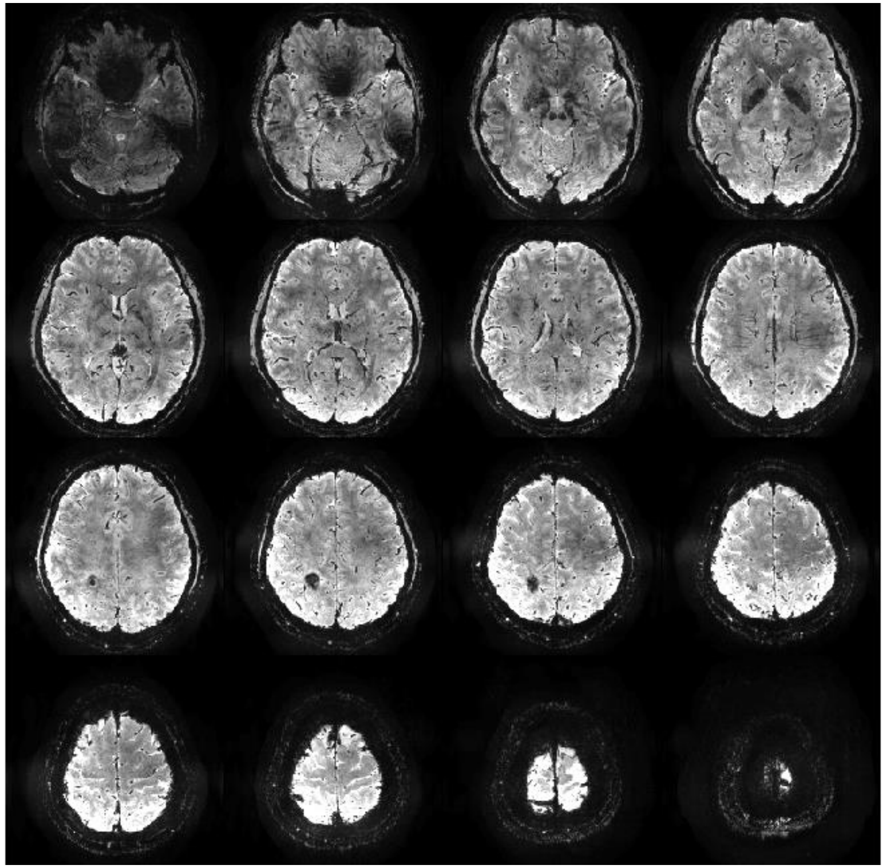

Monique Tourell

Jin Jin

Acknowledgements

Barth Group @ CAI

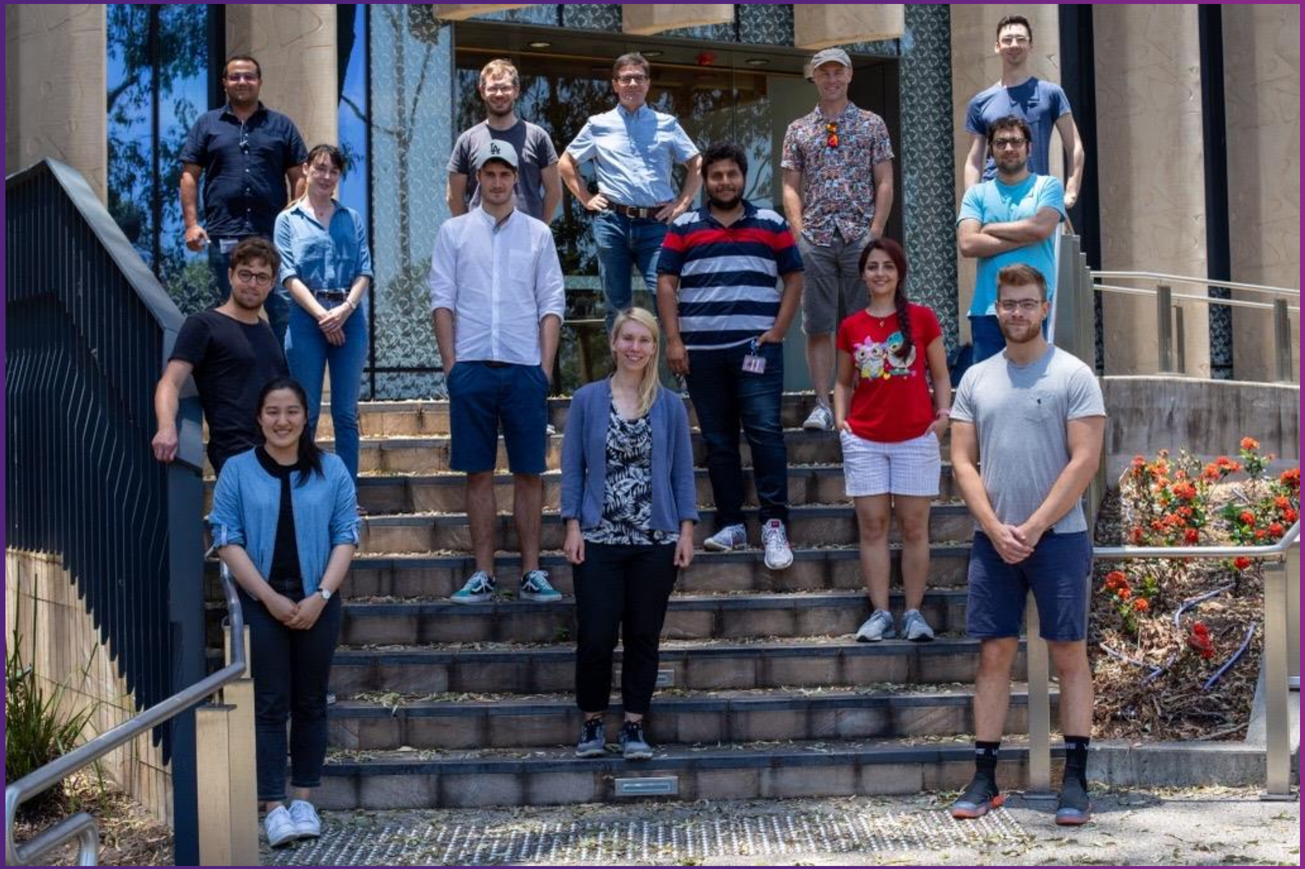

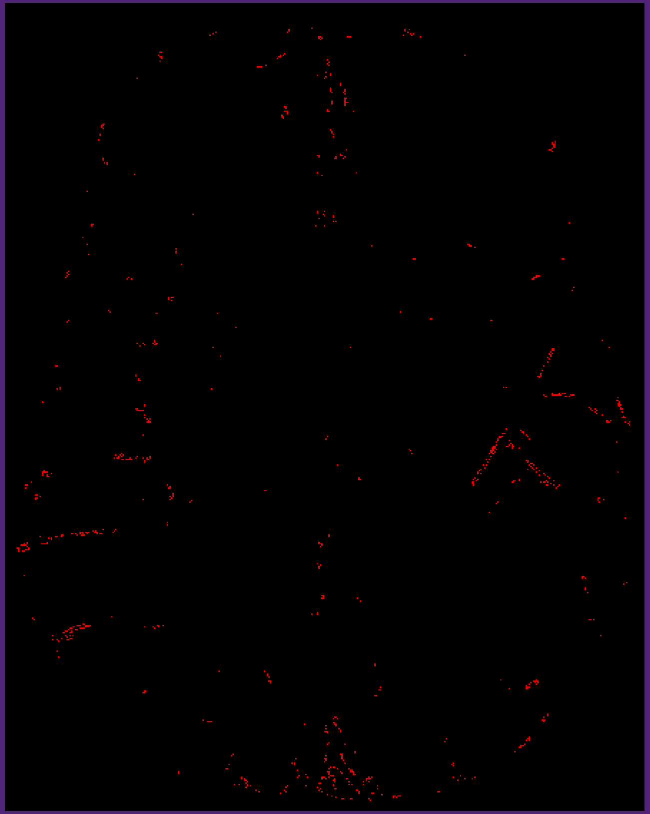

CRICOS code 00025B

ANZ ISMRM Virtual Workshop: Reproducibility tools
20th September 2021 (AEST 10AM)

UHF-MR Symposium (Berlin)
2nd September 2021

mri.sbollmann.net
@sbollmann_MRI

National Imaging Facility

References I

Ahveninen, J., Chang, W.-T., Huang, S., Keil, B., Kopco, N., Rossi, S., Bonmassar, G., Witzel, T., Polimeni, J.R., 2016. Intracortical depth analyses of frequency-sensitive regions of human auditory cortex using 7TfMRI. NeuroImage 143, 116–127. https://doi.org/10.1016/j.neuroimage.2016.09.010

Akbari, A., Bollmann, S., Ali, T.S., Barth, M., 2021. Modelling the depth-dependent VASO and BOLD responses in human primary visual cortex. bioRxiv 2021.05.07.443052. https://doi.org/10.1101/2021.05.07.443052

Amunts, K., Lepage, C., Borgeat, L., Mohlberg, H., Dickscheid, T., Rousseau, M.-É., Bludau, S., Bazin, P.-L., Lewis, L.B., Oros-Peusquens, A.-M., Shah, N.J., Lippert, T., Zilles, K., Evans, A.C., 2013. BigBrain: An Ultrahigh-Resolution 3D Human Brain Model. Science 340, 1472–1475. https://doi.org/10.1126/science.1235381

Barth, M., Norris, D.G., 2007. Very high-resolution three-dimensional functional MRI of the human visual cortex with elimination of large venous vessels. NMR Biomed. 20, 477–484. https://doi.org/10.1002/nbm.1158

Bause, J., Polimeni, J.R., Stelzer, J., In, M.-H., Ehses, P., Kraemer-Fernandez, P., Aghaeifar, A., Lacosse, E., Pohmann, R., Scheffler, K., 2020. Impact of prospective motion correction, distortion correction methods and large vein bias on the spatial accuracy of cortical laminar fMRI at 9.4 Tesla. NeuroImage 208, 116434. https://doi.org/10.1016/j.neuroimage.2019.116434

Besle, J., Sanchez-Panchuelo, R.-M., Bowtell, R., Francis, S., Schluppeck, D., 2013. Single-subject fMRI mapping at 7 T of the representation of fingertips in S1: a comparison of event-related and phase-encoding designs. Journal of Neurophysiology 109, 2293–2305. https://doi.org/10.1152/jn.00499.2012

Bilecen, D., Scheffler, K., Schmid, N., Tschopp, K., Seelig, J., 1998. Tonotopic organization of the human auditory cortex as detected by BOLD-FMRI. Hearing Research 126, 19–27. https://doi.org/10.1016/S0378-5955(98)00139-7

Bollmann, S., Puckett, A.M., Cunnington, R., Barth, M., 2018. Serial correlations in single-subject fMRI with sub-second TR. NeuroImage 166, 152–166. https://doi.org/10.1016/j.neuroimage.2017.10.043

References II

Breuer, F.A., Blaimer, M., Heidemann, R.M., Mueller, M.F., Griswold, M.A., Jakob, P.M., 2005. Controlled aliasing in parallel imaging results in higher acceleration (CAIPIRINHA) for multi-slice imaging. Magn. Reson. Med. 53, 684–691. https://doi.org/10.1002/mrm.20401

Cauley, S.F., Polimeni, J.R., Bhat, H., Wald, L.L., Setsompop, K., 2014. Interslice leakage artifact reduction technique for simultaneous multislice acquisitions. Magn. Reson. Med. 72, 93–102. https://doi.org/10.1002/mrm.24898

Chen, G., Wang, F., Gore, J.C., Roe, A.W., 2013. Layer-specific BOLD activation in awake monkey V1 revealed by ultra-high spatial resolution functional magnetic resonance imaging. NeuroImage 64, 147–155. https://doi.org/10.1016/j.neuroimage.2012.08.060

Chen, J.E., Polimeni, J.R., Bollmann, S., Glover, G.H., 2019. On the analysis of rapidly sampled fMRI data. NeuroImage 188, 807–820. https://doi.org/10.1016/j.neuroimage.2019.02.008

Cheng, K., Waggoner, R.A., Tanaka, K., 2001. Human ocular dominance columns as revealed by high-field functional magnetic resonance imaging. Neuron 32, 359–74. https://doi.org/10.1016/S0896-6273(01)00477-9

Corbin, N., Todd, N., Friston, K.J., Callaghan, M.F., 2018. Accurate modeling of temporal correlations in rapidly sampled fMRI time series. Human Brain Mapping. https://doi.org/10.1002/hbm.24218

de Hollander, G., van der Zwaag, W., Qian, C., Zhang, P., Knapen, T., 2021. Ultra-high field fMRI reveals origins of feedforward and feedback activity within laminae of human ocular dominance columns. Neuroimage 228, 117683. https://doi.org/10.1016/j.neuroimage.2020.117683

Edelstein, W.A., Glover, G.H., Hardy, C.J., Redington, R.W., 1986. The intrinsic signal-to-noise ratio in NMR imaging. Magn. Reson. Med. 3, 604–618. https://doi.org/10.1002/mrm.1910030413

References III

Eklund, A., Andersson, M., Josephson, C., Johannesson, M., Knutsson, H., 2012. Does parametric fMRI analysis with SPM yield valid results?—An empirical study of 1484 rest datasets. NeuroImage 61, 565–578. https://doi.org/10.1016/j.neuroimage.2012.03.093

Engel, S.A., Rumelhart, D.E., Wandell, B.A., Lee, A.T., Glover, G.H., Chichilnisky, E.-J., Shadlen, M.N., 1994. fMRI of human visual cortex. Nature 369, 525–525. https://doi.org/10.1038/369525a0

Feinberg, D.A., Moeller, S., Smith, S.M., Auerbach, E., Ramanna, S., Glasser, M.F., Miller, K.L., Ugurbil, K., Yacoub, E., 2010. Multiplexed Echo Planar Imaging for Sub-Second Whole Brain FMRI and Fast Diffusion Imaging. PLoS ONE 5, e15710. https://doi.org/10.1371/journal.pone.0015710

Fracasso, A., Luijten, P.R., Dumoulin, S.O., Petridou, N., 2018. Laminar imaging of positive and negative BOLD in human visual cortex at 7 T. NeuroImage 164, 100–111. https://doi.org/10.1016/j.neuroimage.2017.02.038

Gagnon, L., Sakad i, S., Lesage, F., Musacchia, J.J., Lefebvre, J., Fang, Q., Yucel, M.A., Evans, K.C., Mandeville, E.T., Cohen-Adad, J., Polimeni, J.R., Yaseen, M.A., Lo, E.H., Greve, D.N., Buxton, R.B., Dale, A.M., Devor, A., Boas, D.A., 2015. Quantifying the Microvascular Origin of BOLD-fMRI from First Principles with Two-Photon Microscopy and an Oxygen-Sensitive Nanoprobe. Journal of Neuroscience 35, 3663–3675. https://doi.org/10.1523/JNEUROSCI.3555-14.2015

Gati, J.S., Menon, R.S., Uğurbil, K., Rutt, B.K., 1997. Experimental determination of the BOLD field strength dependence in vessels and tissue. Magn. Reson. Med. 38, 296–302. https://doi.org/10.1002/mrm.1910380220

Harris, K.D., Mrsic-Flogel, T.D., 2013. Cortical connectivity and sensory coding. Nature 503, 51–58. https://doi.org/10.1038/nature12654

Havlicek, M., Uludağ, K., 2020. A dynamical model of the laminar BOLD response. NeuroImage 204, 116209. https://doi.org/10.1016/j.neuroimage.2019.116209

References IV

Hillman, E.M.C., 2014. Coupling Mechanism and Significance of the BOLD Signal: A Status Report. Annual Review of Neuroscience 37, 161–181. https://doi.org/10.1146/annurev-neuro-071013-014111

Hillman, E.M.C., Devor, A., Bouchard, M.B., Dunn, A.K., Krauss, G.W., Skoch, J., Bacskai, B.J., Dale, A.M., Boas, D.A., 2007. Depth-resolved optical imaging and microscopy of vascular compartment dynamics during somatosensory stimulation. NeuroImage 35, 89–104. https://doi.org/10.1016/j.neuroimage.2006.11.032

Huber, L., Handwerker, D.A., Jangraw, D.C., Chen, G., Hall, A., Stüber, C., Gonzalez-Castillo, J., Ivanov, D., Marrett, S., Guidi, M., Goense, J., Poser, B.A., Bandettini, P.A., 2017. High-Resolution CBV-fMRI Allows Mapping of Laminar Activity and Connectivity of Cortical Input and Output in Human M1. Neuron 96, 1253-1263.e7. https://doi.org/10.1016/j.neuron.2017.11.005

Huber, L., Ivanov, D., Handwerker, D.A., Marrett, S., Guidi, M., Uludağ, K., Bandettini, P.A., Poser, B.A., 2018. Techniques for blood volume fMRI with VASO: From low-resolution mapping towards sub-millimeter layer-dependent applications. NeuroImage 164, 131–143. https://doi.org/10.1016/j.neuroimage.2016.11.039

Iadecola, C., 2017. The Neurovascular Unit Coming of Age: A Journey through Neurovascular Coupling in Health and Disease. Neuron 96, 17–42. https://doi.org/10.1016/j.neuron.2017.07.030

Klein, B.P., Fracasso, A., van Dijk, J.A., Paffen, C.L.E., te Pas, S.F., Dumoulin, S.O., 2018. Cortical depth dependent population receptive field attraction by spatial attention in human V1. NeuroImage 176, 301–312. https://doi.org/10.1016/j.neuroimage.2018.04.055

Kok, P., Bains, L.J., van Mourik, T., Norris, D.G., de Lange, F.P., 2016. Selective Activation of the Deep Layers of the Human Primary Visual Cortex by Top-Down Feedback. Current Biology 26, 371–376. https://doi.org/10.1016/j.cub.2015.12.038

Koopmans, P.J., Barth, M., Norris, D.G., 2010. Layer-specific BOLD activation in human V1. Human Brain Mapping 31, 1297–1304. https://doi.org/10.1002/hbm.20936

References V

Larkman, D.J., Hajnal, J.V., Herlihy, A.H., Coutts, G.A., Young, I.R., Ehnholm, G., 2001. Use of multicoil arrays for separation of signal from multiple slices simultaneously excited. J. Magn. Reson. Imaging 13, 313–317. https://doi.org/10.1002/1522-2586(200102)13:2<313::AID-JMRI1045>3.0.CO;2-W

Lewis, L.D., Setsompop, K., Rosen, B.R., Polimeni, J.R., 2016. Fast fMRI can detect oscillatory neural activity in humans. PNAS 113, E6679–E6685. https://doi.org/10.1073/pnas.1608117113

Lutti, A., Thomas, D.L., Hutton, C., Weiskopf, N., 2013. High-resolution functional MRI at 3 T: 3D/2D echo-planar imaging with optimized physiological noise correction. Magnetic Resonance in Medicine 69, 1657–1664. https://doi.org/10.1002/mrm.24398

Mansfield, P., 1977. Multi-planar image formation using NMR spin echoes. J. Phys. C: Solid State Phys 10. https://doi.org/doi:10.1088/0022-3719/10/3/004

Maudsley, A.A., 1980. Multiple-line-scanning spin density imaging. Journal of Magnetic Resonance (1969) 41, 112–126. https://doi.org/10.1016/0022-2364(80)90207-3

Menon, R.S., Ogawa, S., Strupp, J.P., Ugurbil, K., 1997. Ocular dominance in human V1 demonstrated by functional magnetic resonance imaging. J Neurophysiol 77, 2780–7. https://doi.org/10.1152/jn.1997.77.5.2780

Moeller, S., Yacoub, E., Olman, C.A., Auerbach, E., Strupp, J., Harel, N., Uğurbil, K., 2010. Multiband Multislice GE-EPI at 7 Tesla, With 16-Fold Acceleration Using Partial Parallel Imaging With Application to High Spatial and Temporal Whole-Brain FMRI. Magn. Reson. Med. 63, 1144–1153. https://doi.org/10.1002/mrm.22361

Müller, S., 1988. Multifrequency selective rf pulses for multislice MR imaging. Magnetic Resonance in Medicine 6, 364–371. https://doi.org/10.1002/mrm.1910060315

References VI

Nasr, S., Polimeni, J.R., Tootell, R.B., 2016. Interdigitated Color- and Disparity-Selective Columns within Human Visual Cortical Areas V2 and V3. J Neurosci 36, 1841–57. https://doi.org/10.1523/JNEUROSCI.3518-15.2016

Norris, D.G., 2006. Principles of magnetic resonance assessment of brain function. Journal of Magnetic Resonance Imaging 23, 794–807. https://doi.org/10.1002/jmri.20587

Okada, T., Yamada, H., Ito, H., Yonekura, Y., Sadato, N., 2005. Magnetic field strength increase yields significantly greater contrast-to-noise ratio increase: Measured using BOLD contrast in the primary visual area. Academic Radiology 12, 142–147. https://doi.org/10.1016/j.acra.2004.11.012

Olman, C.A., Harel, N., Feinberg, D.A., He, S., Zhang, P., Ugurbil, K., Yacoub, E., 2012. Layer-Specific fMRI Reflects Different Neuronal Computations at Different Depths in Human V1. PLoS ONE 7, e32536. https://doi.org/10.1371/journal.pone.0032536

Olszowy, W., Aston, J., Rua, C., Williams, G.B., 2019. Accurate autocorrelation modeling substantially improves fMRI reliability. Nature Communications 10, 1220. https://doi.org/10.1038/s41467-019-09230-w

Pohmann, R., Speck, O., Scheffler, K., 2016. Signal-to-Noise Ratio and MR Tissue Parameters in Human Brain Imaging at 3, 7, and 9.4 Tesla Using Current Receive Coil Arrays. Magn. Reson. Med. 75, 801–809. https://doi.org/10.1002/mrm.25677

Polimeni, J.R., Fischl, B., Greve, D.N., Wald, L.L., 2010. Laminar analysis of 7T BOLD using an imposed spatial activation pattern in human V1. Neuroimage 52, 1334–46. https://doi.org/10.1016/j.neuroimage.2010.05.005

Polimeni, J.R., Renvall, V., Zaretskaya, N., Fischl, B., 2018. Analysis strategies for high-resolution UHF-fMRI data. NeuroImage 168, 296–320. https://doi.org/10.1016/j.neuroimage.2017.04.053

References VII

Preibisch, C., G, J.G.C., Bührer, M., Riedl, V., 2015. Evaluation of Multiband EPI Acquisitions for Resting State fMRI. PLOS ONE 10, e0136961. https://doi.org/10.1371/journal.pone.0136961

Pruessmann, K.P., Weiger, M., Scheidegger, M.B., Boesiger, P., 1999. SENSE: Sensitivity encoding for fast MRI. Magnetic Resonance in Medicine 42, 952–962. https://doi.org/10.1002/(SICI)1522-2594(199911)42:5<952::AID-MRM16>3.0.CO;2-S

Puckett, A.M., Bollmann, S., Barth, M., Cunnington, R., 2017. Measuring the effects of attention to individual fingertips in somatosensory cortex using ultra-high field (7T) fMRI. NeuroImage 161, 179–187. https://doi.org/10.1016/j.neuroimage.2017.08.014

Risk, B.B., Kociuba, M.C., Rowe, D.B., 2018. Impacts of simultaneous multislice acquisition on sensitivity and specificity in fMRI. NeuroImage 172, 538–553. https://doi.org/10.1016/j.neuroimage.2018.01.078

Sahib, A.K., Mathiak, K., Erb, M., Elshahabi, A., Klamer, S., Scheffler, K., Focke, N.K., Ethofer, T., 2016. Effect of temporal resolution and serial autocorrelations in event-related functional MRI. Magnetic resonance in medicine 76, 1805–1813.

Sanchez-Panchuelo, R.M., Besle, J., Beckett, A., Bowtell, R., Schluppeck, D., Francis, S., 2012. Within-digit functional parcellation of Brodmann areas of the human primary somatosensory cortex using functional magnetic resonance imaging at 7 tesla. J Neurosci 32, 15815–22. https://doi.org/10.1523/JNEUROSCI.2501-12.2012

Sereno, M.I., Dale, A.M., Reppas, J.B., Kwong, K.K., Belliveau, J.W., Brady, T.J., Rosen, B.R., Tootell, R.B., 1995. Borders of multiple visual areas in humans revealed by functional magnetic resonance imaging. Science 268, 889–893. https://doi.org/10.1126/science.7754376

Setsompop, K., Gagoski, B.A., Polimeni, J.R., Witzel, T., Wedeen, V.J., Wald, L.L., 2012. Blipped-controlled aliasing in parallel imaging for simultaneous multislice echo planar imaging with reduced g-factor penalty. Magn. Reson. Med. 67, 1210–1224. https://doi.org/10.1002/mrm.23097

References VIII

Shamir, I., Assaf, Y., 2021. An MRI-Based, Data-Driven Model of Cortical Laminar Connectivity. Neuroinform 19, 205–218. https://doi.org/10.1007/s12021-020-09491-7

Silver, M.A., Kastner, S., 2009. Topographic maps in human frontal and parietal cortex. Trends in Cognitive Sciences 13, 488–495. https://doi.org/10.1016/j.tics.2009.08.005

Talavage, T.M., Sereno, M.I., Melcher, J.R., Ledden, P.J., Rosen, B.R., Dale, A.M., 2004. Tonotopic Organization in Human Auditory Cortex Revealed by Progressions of Frequency Sensitivity. Journal of Neurophysiology 91, 1282–1296. https://doi.org/10.1152/jn.01125.2002

Tian, P., Teng, I.C., May, L.D., Kurz, R., Lu, K., Scadeng, M., Hillman, E.M.C., De Crespigny, A.J., D'Arceuil, H.E., Mandeville, J.B., Marota, J.J.A., Rosen, B.R., Liu, T.T., Boas, D.A., Buxton, R.B., Dale, A.M., Devor, A., 2010. Cortical depth-specific microvascular dilation underlies laminar differences in blood oxygenation level-dependent functional MRI signal. Proceedings of the National Academy of Sciences 107, 15246–15251. https://doi.org/10.1073/pnas.1006735107

Todd, N., Moeller, S., Auerbach, E.J., Yacoub, E., Flandin, G., Weiskopf, N., 2016. Evaluation of 2D multiband EPI imaging for high-resolution, whole-brain, task-based fMRI studies at 3T: Sensitivity and slice leakage artifacts. NeuroImage 124, 32–42. https://doi.org/10.1016/j.neuroimage.2015.08.056

Triantafyllou, C., Hoge, R.D., Krueger, G., Wiggins, C.J., Potthast, A., Wiggins, G.C., Wald, L.L., 2005. Comparison of physiological noise at 1.5 T, 3 T and 7 T and optimization of fMRI acquisition parameters. NeuroImage 26, 243–250. https://doi.org/10.1016/j.neuroimage.2005.01.007

Ts'o, D., Frostig, R., Lieke, E., Grinvald, A., 1990. Functional organization of primate visual cortex revealed by high resolution optical imaging. Science 249, 417–420. https://doi.org/10.1126/science.2165630

Uğurbil, K., Xu, J., Auerbach, E.J., Moeller, S., Vu, A.T., Duarte-Carvajalino, J.M., Lenglet, C., Wu, X., Schmitter, S., Van de Moortele, P.F., Strupp, J., Sapiro, G., De Martino, F., Wang, D., Harel, N., Garwood, M., Chen, L., Feinberg, D.A., Smith, S.M., Miller, K.L., Sotiropoulos, S.N., Jbabdi, S., Andersson, J.L.R., Behrens, T.E.J., Glasser, M.F., Van Essen, D.C., Yacoub, E., 2013. Pushing spatial and temporal resolution for functional and diffusion MRI in the Human Connectome Project. NeuroImage 80, 80–104. https://doi.org/10.1016/j.neuroimage.2013.05.012

THE UNIVERSITY OF QUEENSLAND AUSTRALIA

References IX

van der Zwaag, W., Francis, S., Head, K., Peters, A., Gowland, P., Morris, P., Bowtell, R., 2009. fMRI at 1.5, 3 and 7 T: Characterising BOLD signal changes. NeuroImage 47, 1425–1434. https://doi.org/10.1016/j.neuroimage.2009.05.015

Wald, L.L., 2012. The future of acquisition speed, coverage, sensitivity, and resolution. NeuroImage 62, 1221–1229. https://doi.org/10.1016/j.neuroimage.2012.02.077

Wandell, B.A., Dumoulin, S.O., Brewer, A.A., 2007. Visual Field Maps in Human Cortex. Neuron 56, 366–383. https://doi.org/10.1016/j.neuron.2007.10.012

Weisskoff, R., Baker, J., Belliveau, J., Davis, T., Kwong, K., Cohen, M., Rosen, B., 1993. Power Spectrum Analysis of Funtionally-Weighted MR Data: What's in the Noise?, in: Proceedings of 12th SMRM Annual Meeting. New York, p. 7.

Weldon, K.B., Olman, C.A., 2021. Forging a path to mesoscopic imaging success with ultra-high field functional magnetic resonance imaging. Philosophical Transactions of the Royal Society B: Biological Sciences 376, 20200040. https://doi.org/10.1098/rstb.2020.0040

Wessinger, C.M., Buonocore, M.H., Kussmaul, C.L., Mangun, G.R., 1997. Tonotopy in human auditory cortex examined with functional magnetic resonance imaging. Human Brain Mapping 5, 18–25. https://doi.org/10.1002/(SICI)1097-0193(1997)5:1<18::AID-HBM3>3.0.CO;2-Q

Worsley, K.J., Friston, K.J., 1995. Analysis of fMRI time-series revisited--again. Neuroimage 2, 173–181. https://doi.org/10.1006/nimg.1995.1023